

MIXED CNT BUNDLE STRUCTURE AND INTERCONNECT ANALYSIS

A DISSERTATION

*Submitted in Partial fulfillment of the
requirements for the award of the degree
of*

MASTER OF TECHNOLOGY

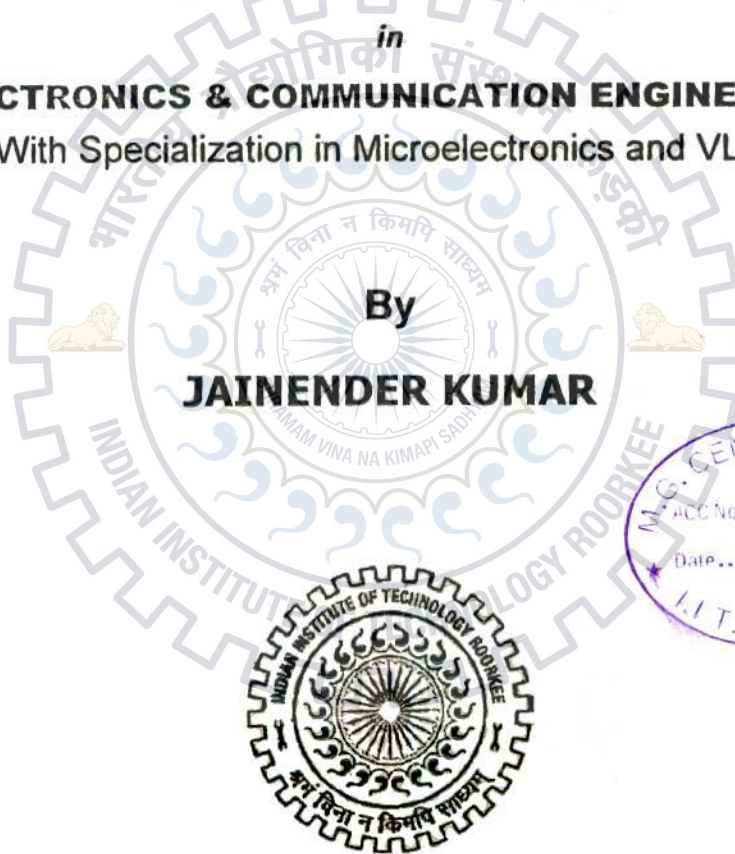
in

ELECTRONICS & COMMUNICATION ENGINEERING

(With Specialization in Microelectronics and VLSI)

By

JAINENDER KUMAR



**DEPARTMENT OF ELECTRONICS AND COMMUNICATION ENGINEERING
INDIAN INSTITUTE OF TECHNOLOGY ROORKEE**

ROORKEE -247 667 (INDIA)

JUNE, 2013

CANDIDATE'S DECLARATION

I hereby declare that the work, which is being reported in this dissertation report, entitled "Mixed CNT bundle structure and interconnect analysis", is being submitted in partial fulfillment of the requirements for the award of the degree of **Master of Technology** in **Microelectronics and VLSI**, in the Department of Electronics and Communication Engineering, Indian Institute of Technology Roorkee, Roorkee is an authentic record of my own work, carried out from June 2012 to June 2013, under guidance and supervision of **Dr. B. K. Kaushik**, Assistant Professor and **Dr. Sudeb Dasgupta**, Associate Professor, Department of Electronics and Computer Engineering, Indian Institute of Technology Roorkee, Roorkee.

The results embodied in this dissertation have not submitted for the award of any other Degree.

Date :

Place : Roorkee



Jainender Kumar

CERTIFICATE

This is to certify that the statement made by the candidate is correct to the best of our knowledge and belief.

Date: 15/6/2013

Place: Roorkee



Dr. B. K. Kaushik

Assistant Professor

Department of E & CE

Indian Institute of Technology, Roorkee



Dr. Sudeb Dasgupta

Associate Professor

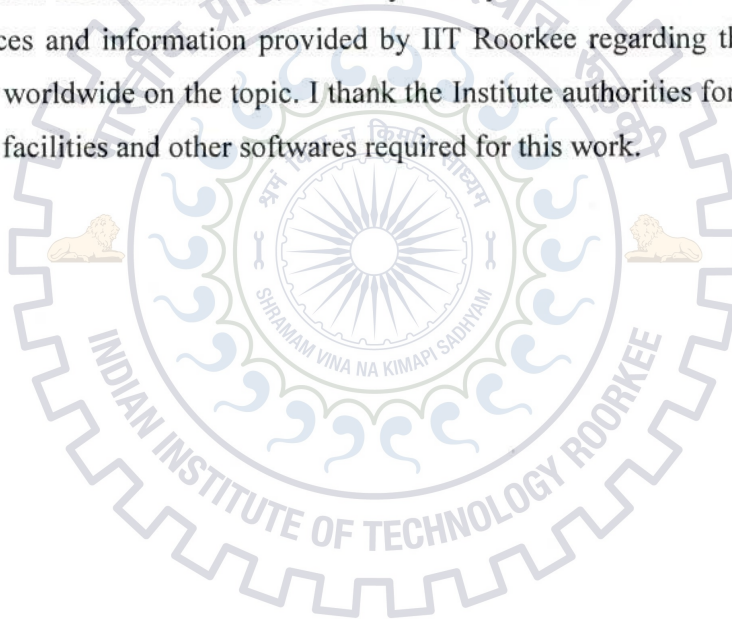
Department of E & CE

Indian Institute of Technology, Roorkee

ACKNOWLEDGEMENT

This dissertation is the end of my journey in obtaining my M.Tech. This journey of mine would have not been completed successfully without the uninterrupted guidance that I receive from my guide Dr. B. K. Kaushik, assistant professor and co-guide Dr. Sudeb Dasgupta, associate professor Department of Electronics and Communication Engineering at Indian Institute of Technology, Roorkee. I would also like to thank Phd. Scholar Mr. Manoj Kumar Majumder for his kind support without whom I could never utilize my skill to this extent.

I owe a huge debt of thanks to the faculty of Microelectronics and VLSI Technology group, department of Electronics and Computer Engineering, IIT Roorkee for their technical assistance and constant motivation to carry out my dissertation. I would like to acknowledge the resources and information provided by IIT Roorkee regarding the research work being conducted worldwide on the topic. I thank the Institute authorities for granting me the use of laboratory facilities and other softwares required for this work.



Jainender Kumar

M.Tech (MEV)

ABSTRACT

International Technology Roadmap for Semiconductor (ITRS) realizes the fact that Cu interconnect does not hold properties required to match the coming era of nano-technology. A new interconnect material is required that can hold current density of 3.3×10^6 A/cm² as per ITRS. Carbon nanotubes (CNT) during the research phase proved to be the best material suited for VLSI interconnect technology. It has unmatched electrical, mechanical, thermal and chemical properties.

CNTs are classified as single and multi-walled CNTs that can be deployed as single or bundled arrangement. Bundled CNT is preferred as it decreases the contact resistance to a great extent as compared to single CNT, offering a great improvement in performances. Realizing a pure SWCNT or pure MWCNT bundle is a difficult task due to the limitation involved in process control techniques and fabrication technology. However, a CNT bundle having different diameter CNTs is more appreciated from the fabrication point of view. In fact, mixed CNT bundle (MCB) is the natural bundle available post fabrication wherein outer diameter of CNTs follows Gaussian distribution. MCB is yet to be researched for its unparalleled performance in terms of propagation delay, power dissipation and crosstalk delay.

Advancement in technology results in shrinking of device dimension that causes densely packed ICs. Therefore, it becomes increasingly difficult to fabricate a nanoscale IC with exact geometry. It results in considerable deviations of their performance. This deviation can cause logic failure that is caused by uncertainties in propagation delay from its mean value. In this dissertation report monte carlo simulations method is implemented on different CNT bundles to analyse the process induced variation on interconnect parameters as delay, crosstalk and power dissipation.

TABLE OF CONTENTS

Candidate's Declaration	ii
Acknowledgement	iii
Abstract	iv
Table of Contents	vi
List of Figures	vii
List of Tables	ix
1 Introduction	1
1.1 Classification of Carbon Nanotubes.....	2
1.1.1 Single-Walled Carbon Nanotubes (SWCNT)	2
1.1.2 Double –Walled Carbon Nanotube (DWCNT)	3
1.1.3 Multi-Walled Carbon Nanotubes (MWCNT)	3
1.2 Structure of CNT.....	4
1.3 Properties.....	5
1.3.1 Electrical.....	5
1.3.2 Thermal.....	7
1.3.3 Mechanical	7
1.3.4 Chemical.....	8
1.4 Application.....	8
1.5 Motivation of the Thesis	9
1.6 Organisation of the Thesis.....	10
2 Equivalent <i>RLC</i> Model of Mixed CNT Bundle	11
2.1 Specific Arranged MCB Interconnect Model	12
2.1.1 Model-I	12
2.1.2 Model-II.....	15
2.2 <i>RLC</i> Circuit Modelling of Randomly Arranged MCB	19
2.2.1 Model-III.....	19

3 Performance Analysis	27
3.1 Simulation Setup	27
3.2 Crosstalk and Power dissipation Analysis using Model-I.....	28
3.3 Propagation delay Analysis using Model-II.....	31
3.3.1 MWCNT	31
3.3.2 MWCNT Bundle.....	31
3.3.3 MCB.....	33
3.4 Propagation, Power dissipation and Crosstalk delay Analysis using Model-III	35
3.4.1 Transient Analysis of MTL and ESC.....	35
3.4.2 Propagation delay and power dissipation	37
3.4.3 Crosstalk	38
4 Process variation in MCB	41
4.1 Process Induced Variation.....	41
4.1.1 Temperature	42
4.1.2 Metallic ratio	43
4.1.3 Contact resistance	44
4.1.4 Bundle Area	45
5 Conclusion and Future work	47
5.1 Conclusion.....	47
5.2 Future work	48
References	49
Publications	53

List of Figures

Figure 1.1 Allotropes of carbon (a) Fullerenes (C_{60}) (b) Graphene [4].....	1
Figure 1.2 Single SWCNT Structure [7].....	2
Figure 1.3 DWCNT Structure.....	3
Figure 1.4 MWCNT Structure.....	4
Figure 1.5 CNT structure showing the vectors a_1 and a_2 in Zig Zag and Armchair with chirality (3,3) [13].	5
Figure 1.6 Structure showing SWCNTs having (a) armchair ($n=m$), (b) zig-zag (n or $m =0$), and (c) chiral chirality [12]	5
Figure 1.7 Energy band diagram showing valence and conduction band [9].....	6
Figure 2.1 Physical structures of possible specific arranged MCB (a) SWCNT bundle, (b) DWCNT bundle, (c) MCB having randomly arranged CNTs, (d) MCB with half SWCNTs and half DWCNTs and, (e) MCB half occupied with SWCNT and half with MWCNTs(c).....	11
Figure 2.2 Equivalent RLC model of MCB.....	13
Figure 2.3 MTL model of distributed RLC network of MWCNT [7].	15
Figure 2.4 ESC distributed RLC circuit model of MWCNT.	16
Figure 2.5 Figure showing MCB structure with (a) MWCNT in outer periphery and SWCNT filled inside and (b) SWCNT in outer periphery with MWCNT filled inside.	19
Figure 2.6 Geometry of SWCNT and MWCNT above ground plane	20
Figure 2.7(a) Tube density variation for different mean diameter of CNTs and (b) Gaussian distribution of CNTs having different mean diameters	21
Figure 2.8 MTL model of MCB	24
Figure 2.9 ESC model of MCB.....	25
Figure 3.1 Simulation setup for MWCNT interconnects with CMOS inverter used as driver	27
Figure 3.2 Two-line bus architecture of CNTs [21]	28
Figure 3.3 Crosstalk for different interconnect lengths for different bundled CNT structures.	29
Figure 3.4 Power dissipations for different bundle structure at different lengths	29
Figure 3.5 Propagation delay with varying interconnect lengths for bundled MWCNT that has the area of (a) $12 \times 24 \text{ nm}^2$ (b) $28 \times 56 \text{ nm}^2$, & (c) $44 \times 90 \text{ nm}^2$	33

Figure 3.6 CNT Bundle showing (a) MCB-III and (b) MCB-IV [8].....	33
Figure 3.7 Propagation delay variation of MCB-III and MCB-IV for various interconnect length.....	34
Figure 3.8 Output voltage waveforms at different interconnect lengths of (a) 10 μ m, (b) 50 μ m, (c) 100 μ m and (d) 400 μ m, computed by means of an exact MTL formulation and a reduced ESC approach	36
Figure 3.9 Propagation delay variation for different (a) D_R and (b) interconnect lengths.....	39
Figure 3.10 Propagation delay and power dissipation for different number of tubes in a MCB	39
Figure 3.11 Crosstalk delays for different tube density in a MCB	39
Figure 4.2 Average deviation in delay with different interconnect lengths for process induced temperature variation	43
Figure 4.3 Average deviation in delay with different interconnect lengths for process induced metallic ration variation	44
Figure 4.4 Average deviation in delay with different interconnect lengths for process induced contact resistance variation	45
Figure 4.5 Average deviation in delay with different interconnect lengths for process induced bundle area variation	46

List of Tables

Table 1.1 Comparison between different properties of Cu, SWCNT, MWCNT and graphene [5]	8
Table 2.1 Diameters and Corresponding number of CNTs for different Bundle density	23
Table 2.2 Numbers and Corresponding Diameters of SWCNTs and MWCNTs in a MCB (Bundle Area= $4\mu\text{m}^2$) for Different Values of D_R	23
Table 2.3 Diameters and Corresponding number of CNTs for different Bundle density	24
Table 2.4 Numbers and Corresponding Diameters of Swcnts and Mwcnts in a MCB (Bundle Area= $4\mu\text{m}^2$) for Different Values of D_r	24
Table 3.1 Improvement in Crosstalk for MCB-II w.r.t. Other bundled CNT structures	30
Table 3.2 Percentage improvement in power dissipation for MCB-II w.r.t. other bundled CNT structures	30
Table 3.3 Equivalent interconnect parasitic for different Bundled CNT Structures	30
Table 3.4 Comparison of propagation delay between reference model [9] and proposed esc model	32
Table 3.5 Propagation Delay for Different MWCNT Bundle Areas at Global Interconnect Lengths	32
Table 3.6 Propagation delay (in ns) for different interconnect length.....	34
Table 3.7 Propagation delays at Different interconnect lengths	36
Table 3.8 Interconnect Parasitics for Different Bundle Density	37
Table 3.9 Variation of Mean Diameter for Realistic MCB with a Fixed Bundle area of $4\mu\text{m}^2$	38
Table 4.1 Parameter Variation/Range	42
Table 4.2 Propagation Delay for different CNT Bundles	42
Table 4.3 Interconnect parasitics for Process Induced Temperature variation	43
Table 4.4 Interconnect Parasitics for Process Induced Metallic Ration variation	44
Table 4.5 Interconnect parasitics for Process Induced contact resistance variation	45
Table 4.6 Interconnect parasitics for Process Induced Bundle Area variation	46

1 Introduction

Carbon has an unmatched ability to bond with itself and with other atoms in endlessly varied combinations of chains and rings making it an interesting and popular material among researchers. Sumio Iijima, viewed as the inventor of carbon nanotubes, ignited a special interest in the field of carbon nanostructures [1]. Since the year of 1991, a lot of researches have been carried out in the area of nanotechnology. Two German scientist L. V. Radushkevich and V. M. Lukyanovich in 1952 issued images of carbon nanotubes having 50nm diameter as reported in the *Soviet Journal of Physical Chemistry* [2]. This discovery was overlooked because the journal was in the Russian language and access to Soviet press by any western scientist was prohibited due to the cold war. Carbon nanotube is one of the discoveries from the class of fullerenes. Every fullerene like C_{60} , C_{70} , C_{84} , etc. have basic but similar pure carbon cage characteristic, where each atom is bonded to three other atoms just like in graphite [3]. However, fullerenes are different form of graphite in the sense that each fullerene has precisely 12 pentagonal faces having different number of hexagonal faces (e.g. C_{60} has 20). Structure of C_{60} is spherical just like ball with 32 faces. Out of the 32 faces, 12 are pentagons and 20 hexagons similar to a soccer ball as shown in Fig. 1.1(a). Carbon atoms not only have the property to form soccer shaped molecules but also exists in long cylindrical tubes. These new form of long cylindrical tubes are called buckytubes which is now also known as carbon nanotubes (CNTs) [4].

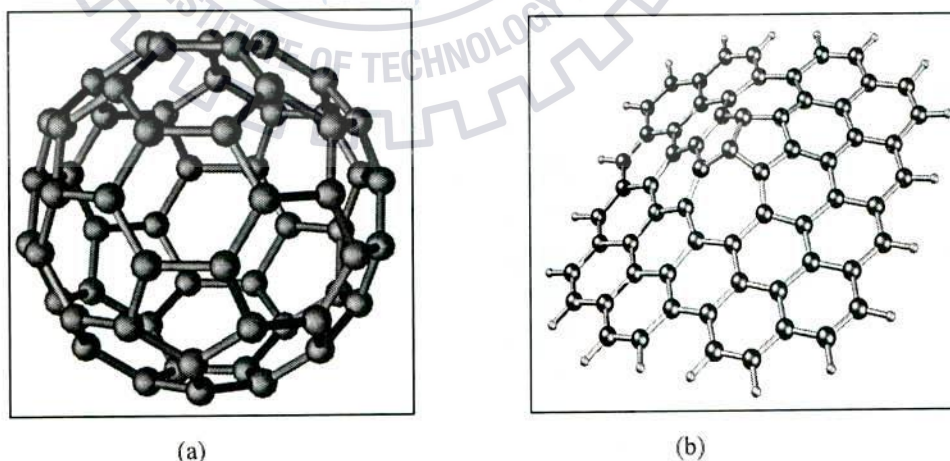


Figure 1.1 Allotropes of carbon (a) Fullerenes (C_{60}) (b) Graphene [4]

Carbon atom has various allotropes due to its extremely high linking property that exists as three, two, one and zero dimensional structure that are listed as follows:

- Three dimensional :- Diamond and Graphite
- Two dimensional :- Graphene
- One dimensional :- Graphene Nano ribbon
- Zero dimensional :- Fullerenes

1.1 Classification of Carbon Nanotubes

CNTs are basically formed by rolling of graphene sheets into cylindrical form [4], and thus can be classified as follows

- 1) Single Walled Carbon Nanotube (SWCNT)
- 2) Double Walled Carbon Nanotube (DWCNT)
- 3) Multi Walled Carbon Nanotube (MWCNT)

1.1.1 Single-Walled Carbon Nanotubes (SWCNT)

Single-wall carbon nanotube (SWCNT) comprises of single cylindrical layer of graphite having one atom thickness rolled to form cylinder having high aspect ratio as shown in Fig. 1.2. SWCNT having diameter in the range of 0.8nm to 1nm is said to exhibit electrical stability and good electrical conductivity [6]. Contrary to diameter, the length of CNTs can be thousands times longer than its diameter. SWCNTs are more flexible as compared to MWCNTs but are not trivial to fabricate. Due to its better flexibility, they can be bent into circular fashion, twisted and flattened without any damage. SWCNTs have unique electrical and mechanical properties that find usage in various applications, such as logic elements, nanosensors, nanocomposite materials, and field-emission displays [7].

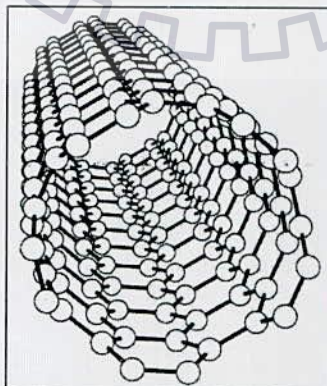


Figure 1.2 Single SWCNT Structure [7]

1.1.2 Double–Walled Carbon Nanotube (DWCNT)

Double-wall carbon nanotubes (DWCNTs) are classified as special type of MWCNT wherein two concentrically graphene sheets are rolled up as shown in Fig. 1.3. The properties of DWCNT are similar to that of a SWCNT and an MWCNT. They are significantly tolerant to chemicals as the outer shell shields the inner shell. DWCNTs are flexible as SWCNTs while maintaining the electrical and thermal property of MWCNTs. DWCNTs can be thought as a mixture of both SWCNT and MWCNT. Due to the perfect blend, they have acquired highly specific applications. SWCNTs are highly susceptible to breakage as the foreign particles can have direct contact with outer shell that can significantly alter the properties. On the other hand, DWCNTs have two shells wherein outer shell provides shielding to the inner shell and hence intrinsic properties are preserved. Due to shielding property DWCNT provide better thermal and chemical stability than SWCNT. DWCNTs also find usage in various applications like field-emission displays, nanocomposite materials, and nanosensors.

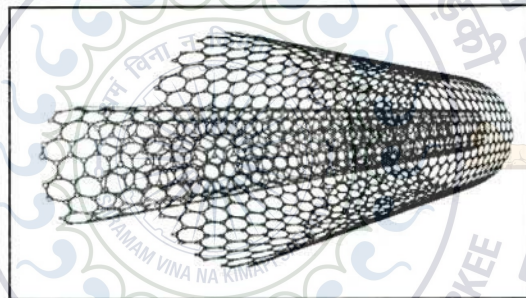


Figure 1.3 DWCNT Structure

1.1.3 Multi-Walled Carbon Nanotubes (MWCNT)

Multi-wall carbon nanotube (MWCNT) consists of several concentric shells having different diameters. Each shell in MWCNT exhibits different electrical and physical properties. MWCNTs with diameter higher than 20nm have band gap lesser than thermal energy making them conductive at room temperature ($E_G < k_B T \approx 0.0258\text{eV}$) [9]. The number of conducting channels and mean free path increase is directly proportional to the diameter of MWCNTs [10] due to which higher diameter MWCNT exhibits better performance in comparison to the MWCNT having smaller diameter. MWCNT bundle is preferred over single MWCNT or SWCNT bundle as it provides greater number of conducting channels.

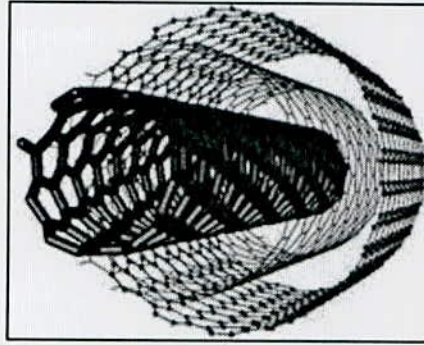


Figure 1.4 MWCNT Structure

1.2 Structure of CNT

CNTs are known as allotropes of carbon. An isolated carbon atom has four electrons valence band distributed among atomic orbitals $2s$, $2p_x$, $2p_y$, and $2p_z$ respectively. In contrast, carbon atom in graphene have three atomic orbitals $2s$, $2p_x$, and $2p_y$ that are hybridized to form three coplanar sp^2 orbitals while the $2p_z$ orbital is perpendicular to it. The three hybridized orbitals forms sigma (σ) bond that is responsible for bonding between the adjacent carbon atoms whereas $2p_z$ orbital forms π bonds out of the plane of graphene [11]. The strong sp^2 bonding in graphene makes CNTs as strongest material even if compared to the sp^3 bonding of diamond [11]. Structure of CNTs depend on rolling up direction of graphene sheets defined by chiral indices (n, m) . Chiral vectors decide whether the CNT is metallic or semiconducting in nature. Furthermore, CNTs can also be classified as armchair and zigzag structure depending on their chiral indices (n, m) . For armchair, chiral indices are equal and defined as $n = m$ and for zigzag, it is n or $m = 0$ [5]. CNTs satisfying the condition $n - m = 3i$ (where i is an integer) are termed as metallic and thus armchair CNTs are always metallic and zigzag CNTs can be either metallic or semiconducting in nature [12].

The structure of CNT can be defined using their circumferential vector as [13]

$$\vec{C} = n \cdot a_1 + m \cdot a_2 \quad (1)$$

where a_1 and a_2 denotes the unit vectors. The diameter of CNT can be calculated using the chiral vectors as [5]

$$D = \frac{|\vec{C}|}{\pi} = \frac{a}{\pi} \sqrt{n^2 + m^2 + nm} \quad (2)$$

As discussed, the chiral vector decides the property of CNTs. Chirality decides the metallic and semiconducting nature of CNTs. It also effects the other properties such as conductance, lattice structure, density etc.

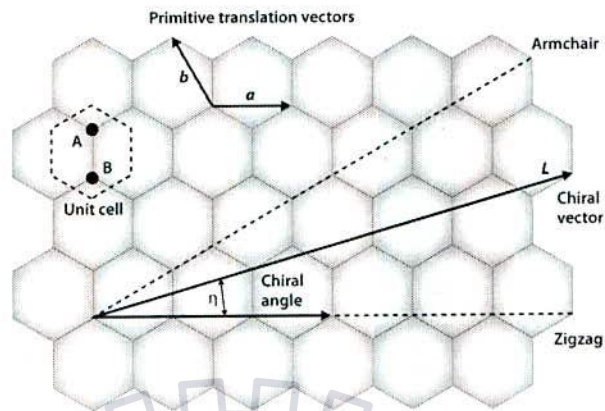


Figure 1.5 CNT structure showing the vectors a_1 and a_2 in Zig Zag and Armchair with chirality (3,3) [13]

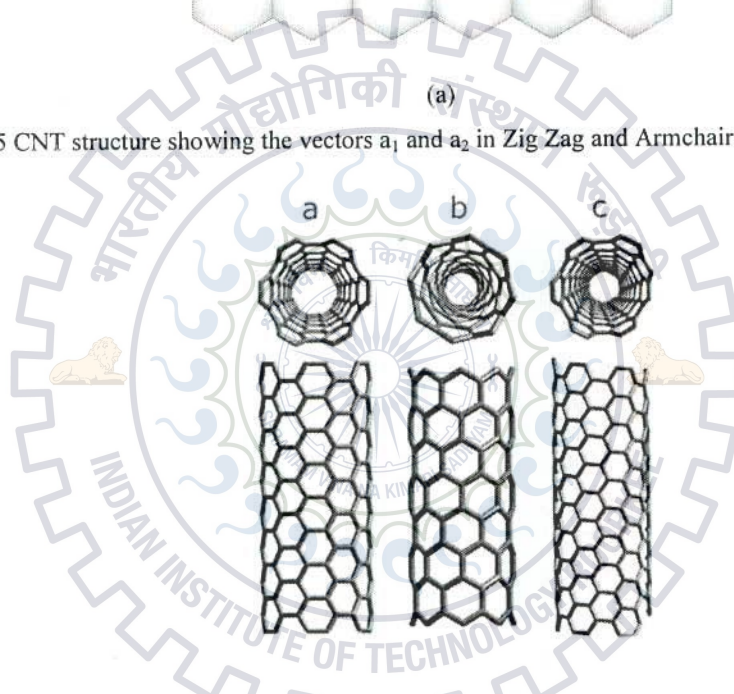


Figure 1.6 Structure showing SWCNTs having (a) armchair ($n=m$), (b) zig-zag (n or $m=0$), and (c) chiral chirality [12]

1.3 Properties

CNTs have unique electrical, thermal, mechanical and chemical properties that make CNTs one of the promising candidates in global VLSI interconnects. These extraordinary physical properties are listed as follows:

1.3.1 Electrical

Electronically, CNTs are classified as semiconducting and metallic, depending on $(n-m)$ value. The equivalent value of $(n-m)$ is either zero or multiple of three, which indicates that

they have electrons in their valence band at room temperature and are metallic in nature. Other possible values of $(n-m)$ exhibits the semiconducting nature of CNTs. Semiconducting CNTs have band gap ranging from 0.25eV to 3.5eV [16]. Band gap is an inverse function of diameter and thus higher diameter indicates the reduction in band gap and vice-versa. For an instance, CNTs having tube diameter of 1nm have band gap of about 1eV [16].

There are a lot of electrons that occupies different energy levels within the nanotube. Fig. 4 shows the energy band diagram for a single CNT. The shaded area corresponds to the valence band and indicated the state filled with electrons, whereas the unshaded area corresponds to the conduction band and signifies the energy levels that an electron can occupy. A photon having energy higher than the band gap of CNTs can be easily absorbed causing electron to take transition from valence band to conduction band. Photo absorptions in CNTs produce characteristic absorption spectrum in the range of ultraviolet to near-infrared wavelength [11]. By observing the light absorption, one can identify the range of (m, n) of a given tube.

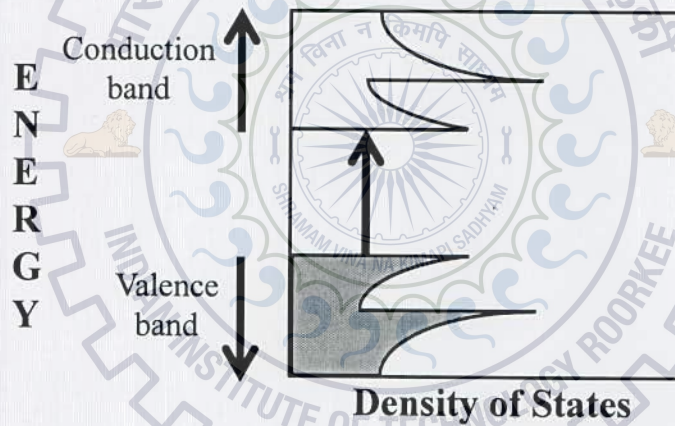


Figure 1.7 Energy band diagram showing valence and conduction band [9]

As the conductivity of CNT is very high electrons and holes can move very easily. The predicted value of nano-sized Cu is equal to the electrical resistance offered by single CNTs. When CNTs are tied together as a bundle (CNT bundle), generally electron flow across the CNTs but sometimes due to tunnelling phenomenon the electron jumps from one CNT to other. Resistivity of CNT bundle can be as low as 10^{-4} ohm-cm at room temperature [17]. This makes the CNTs highest conductive material known.

The electrons in the CNT are highly polarizable due to which energy level largely depends on environment. Electrons under the influence of external field can enhance or degrade the

conductivity by shifting the relative energies. This makes CNTs useful as printable semiconductor in transistor applications.

Similarly there are several molecules other than photon that can shift energy levels affecting the conductivity and optical behaviour as well. Degree in shift in energy levels depends on the type of molecule attached to the CNT. This property can help the CNTs to find usage in sensor application or bio medics. Every molecule will shift the energy levels differently hence can be recognized easily.

In CNTs, the conduction of electrons are ballistic in nature. In ballistic region, the electron flowing inside the CNT does not experience any scattering. This region ranges to several micron which is thousand times larger than Cu [18]. Ballistic region allows considerable amount of current flow without much heat generation. This helps the CNTs to handle enormous amount of current density without any sign of damage. In fact, CNTs are reported to have highest current density of 10^9 A/cm² that is 100 times more that of Cu. Conductivity of different types of CNTs with other properties is shown Table I.

1.3.2 Thermal

Diamond was considered as the best thermal conductor before the discovery of CNTs. Along the axis, CNTs are reported to have thermal conductivity of about 3000 Watts per meter-degree Kelvin [19]. For comparison, the diamond has thermal conductivity in between 900 and 2300W/m-K [20], while copper has 400W/m-K [21]. CNTs show better thermal conductivity only along the axis in comparison to the conductivity in transverse direction. It is observed that the conductivity in transverse direction is reduced by a factor of 100. It is due to the fact that vibrations of carbon atoms find it easily to propagate down the tube. In transverse direction it is more rigid. Due to high thermal conductivity, CNTs can be used to carry away heat from electronics circuitry enabling another usage in ultra-small circuits.

1.3.3 Mechanical

CNT has Young's modulus of upto 1.4TPa making it the strongest fibre known [22]. CNT is reported to have a tensile strength of 50Gpa [23]. For comparison, high strength steel has Young's modulus of about 200Gpa and tensile strength 1-2Gpa respectively which is much smaller as compare to CNT. With such stiffness CNTs can be bent over or twisted without any damage which shows quite a remarkable property.

1.3.4 Chemical

CNTs as discussed earlier have remarkable property to form countless combinations and derivatives of carbon atom. CNT inherently possesses all the properties of carbon. Many synthetic structures are possible with nanotubes that are not possible with any other carbon structure. They are as follows

1. Functional group attach at both the ends of CNT can communicate via CNT providing true metallic transport of electron.
2. Molecules attach to the CNT with covalent bind provides chemical handle that allow manipulation of tube and also helps it to attach other things. MWCNTs allow functionalization of external walls/shells without altering the intrinsic property.

CNT has the property to combine with other molecules either covalently or non-covalently. In covalent bond both CNT and molecules share an electron whereas in non-covalent bond other molecule simply attach to the outer side walls of CNT. The non-covalent bond provides a type of nano-scale coating to the CNT. Due to polarization behaviour of CNT, the molecule attaching non-covalently causes significant changes in the electronic structure. Because the sidewalls of CNT is electrically polar in which molecules find is easy adhere to their surfaces. When molecules adhere non-covalently to the CNT surface, they often cause subtle changes in the electronic structure of the tubes. These changes are detectable and hence make CNT sensitive to chemicals. Due to this property CNTs can be used as chemical sensors [7].

Table 1.1 Comparison between different properties of Cu, SWCNT, MWCNT and graphene [5]

Properties	Cu	SWCNT	MWCNT	GRAPHENE
Max current density (A/cm ²)	>10 ⁷	>10 ⁹	>10 ⁹	>10 ⁸
Melting point (K)	1356	3800 (graphite)		
Thermal conductivity (X 10 ³ W/m-K)	0.385	1.75 - 5.8	3	3 - 5
Temperature Coefficient of resistance (X 10 ⁻³ / K)	4	<1.1	-1.37	-1.47
Mean free path @ room Temperature	40	<10 ³	2.5 X 10 ⁴	10 ³

1.4 Application

CNTs due to its extraordinary properties in all respect find usage in various applications, some of them are listed [24] as

- **Electronics:** Interconnects, Digital electronics, Transistors, CNT-FET, RF circuits, Nano electronics.
- **Electrical:** Electrostatic discharge (ESD), Electrical shielding, Electromagnetic interference (EMI) and Electrical cables and wires.
- **Thermal:** Heat sink and on chip thermal management.
- **Energy applications:** Electrode material, Conductive filter, Storage device, Super capacitor, Li-ion battery, Solar cell and Fuel cell.
- **Mechanical:** Load bearing enforcement in composite, Digital electronics, Super capacitors, Tennis racket, Spacecraft and Aircraft body parts.
- **Biological:** Imaging application within live cell and tissues and carrier to therapeutic drugs.

1.5 Motivation of the Thesis

As per the International Technology Roadmap for Semiconductors (ITRS) [25], for upcoming interconnect technology, it is required to design high-speed interconnect that have smaller wire width and longer length [26]. Thus, Cu interconnects have suffered from electromigration [27] [28] and increased in propagation delay due to several parasitic effects [25]. CNTs are believed to be one of the interconnect material capable to cope with the shrinking nano-scale technology due to its extraordinary physical properties. Pure SWCNT and MWCNT bundle is impractical to realize due to limitations and cost effective parameters associated with current diameter controlling methods [29]. Therefore, a natural bundle having different types of CNTs can be preferred for future VLSI interconnects [30] [10]. Due to less complexity involved in fabrication, a mixed CNT bundle (MCB) is proposed in which SWCNTs, DWCNTs and MWCNTs are randomly arranged.

In existing literatures [10] [9] [30], it is difficult to find the exact modelling of MCB that truly replicates the behaviour of MCB. Therefore, this dissertation work has introduced the modelling of interconnect parasitics using specified and random arrangements of SWCNTs, DWCNTs and MWCNTs in a bundle. The proposed bundle arrangements are further used to analyze different performances such as propagation delay, crosstalk and power dissipation. Moreover, the randomly arranged MCBs are modelled to demonstrate the effect of process induced parameter variations.

1.6 Organisation of the Thesis

The thesis is organized as follows:

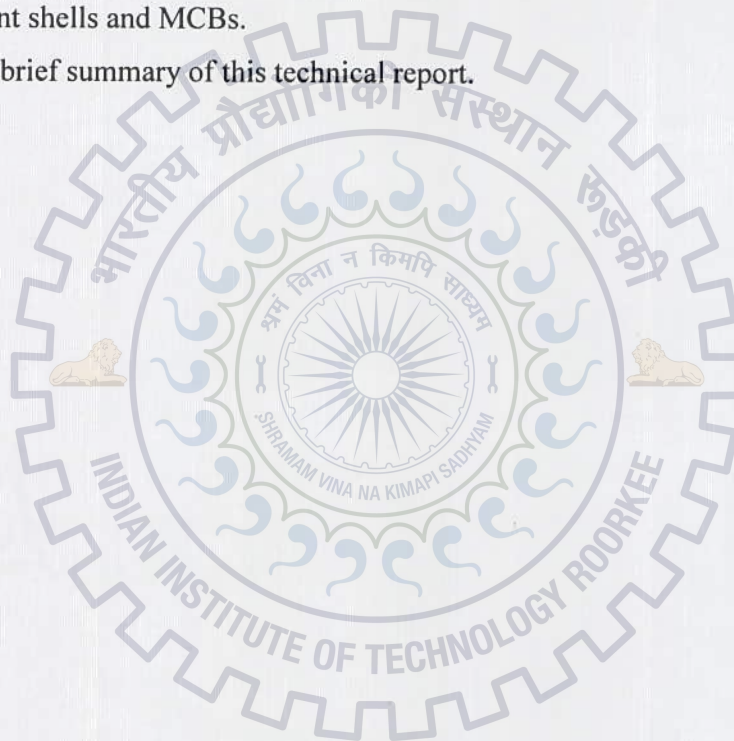
Chapter 1: Presents the introduction about the CNTs. A brief analysis of their properties, structures and applications are demonstrated in this chapter.

Chapter 2: Presents different *RLC* models for MCB interconnects. The modelling is carried out based on the multi-conductor transmission line theory that takes into accounts the effect of diameter dependent mean free paths.

Chapter 3: Analyzes the impact on propagation delay, power dissipation and crosstalk for different MCB configurations.

Chapter 4: Presents the impact of process variations among SWCNT bundle, MWCNT bundle having different shells and MCBs.

Chapter 5: Draws a brief summary of this technical report.



2 Equivalent RLC Model of Mixed CNT Bundle

This chapter contains the modelling of different types of mixed bundle based on arrangement of CNTs in it. The CNT bundle modelling is basically divided according to the arrangement of CNTs inside bundle that are categorizes as

1. Specific arrangement of MCB.
2. Random arrangement of MCB.

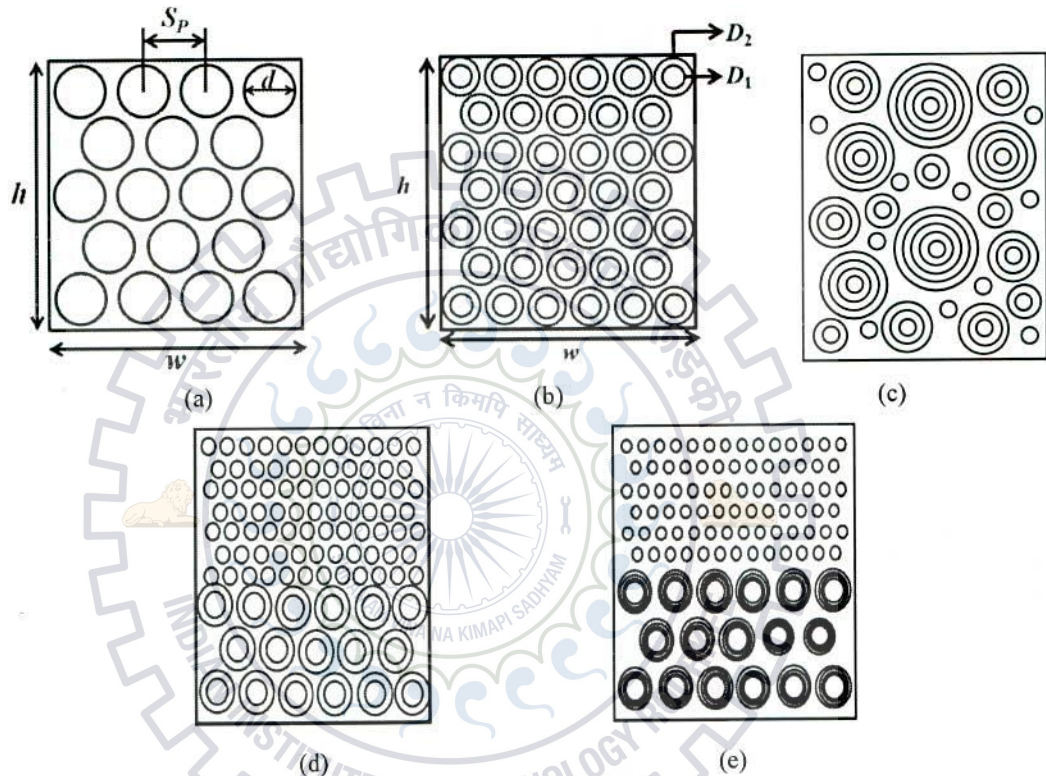


Figure 2.1 Physical structures of possible specific arranged MCB (a) SWCNT bundle, (b) DWCNT bundle, (c) MCB having randomly arranged CNTs, (d) MCB with half SWCNTs and half DWCNTs and, (e) MCB half occupied with SWCNT and half with MWCNTs(c)

In specific arranged bundle CNTs inside the MCB are arranged in specific manner and structure is deterministic. The calculation involved in calculating the number of CNTs of different kind is simple as compared to random arranged MCB.

In randomly arranged MCB structure is random and is probabilistic in nature. Random structure is complex and distribution of CNTs inside the MCB is in accordance with outer diameter of a CNT following Gaussian distribution.

2.1 Specific Arranged MCB Interconnect Model

In this section modelling of specific arranged MCB is proposed based on the structure of MCB. On the basis of geometry of MCB, distributed RLC parameters have been evaluated and their equivalent circuit models are derived. RLC modelling is done on the basis of transmission line theory and T structured transmission line is followed.

2.1.1 Model-I

The structures of bundled SWCNT and bundled DWCNT are shown in Fig. 2.1(a) and 2.1(b) respectively. As presented in Fig. 2.1(a), bundled SWCNT constitutes a number of SWCNTs having d and S_p as diameter and spacing respectively [31] [32].

$$n_{CNT} = \begin{cases} n_H n_W - (n_W/2) & , n_H \text{ is even} \\ n_W n_H - \left[\frac{n_W - 1}{2} \right] & , n_H \text{ is odd} \end{cases} \quad (3)$$

where

$$n_W = w / (d + S_p) \quad \text{and} \quad n_H = h / (d + S_p) \quad (4)$$

n_W , n_H , n_{CNT} , h and w represents the number of CNTs across the horizontal and vertical side of bundle, total number of SWCNTs in a bundle, bundle height and width respectively. Similarly, Fig. 2.1(b) shows bundled DWCNT structure of width w and height h that contains number of DWCNTs. Each DWCNT has two shells with diameters D_1 and D_2 , where D_1 and D_2 are the diameter of inner and outer shell respectively. Distance between the two shells (intershell spacing S_i) is fixed whereas outermost diameter can have values depending on number of shells. Intershell spacing S_i can be expressed as [9]

$$S_i = \frac{D_2 - D_1}{2} \approx 0.34nm \quad (5)$$

Based on the arrangements of different CNTs in a bundle, two novel MCB structures such as MCB-I and MCB-II are proposed as shown in Figs. 2.1(d) and 2.1(e) respectively. SWCNTs and DWCNTs occupy equal halves with horizontal arrangements in MCB-I structure. MCB-II also has the similar arrangement except that the types of CNTs used are the SWCNTs and MWCNTs.

A. Equivalent RLC Model

Equivalent RLC model of MCB is combination of the equivalent models of bundled SWCNT and bundled MWCNT interconnects. Equivalent RLC models for bundled CNTs are developed by considering three different levels in the bundle: (1) the number of CNTs in first bottom level is considered as N_A which is equal to n_W , (2) the second level in bundle consists of N_B number of CNTs that can be presented as

$$N_B = N_A - 1 \quad (6)$$

(3) the numbers of CNTs in rest of the levels are considered as N_C that is equal to

$$N_C = n_H - N_A - N_B \quad (7)$$

Using the novel modelling approach, equivalent RLC of MCB interconnect is presented in Fig. 2.2 that contains equivalent models of bundled SWCNT and bundled MWCNT interconnects. Bundled MWCNT and DWCNT have a number of MWCNTs and DWCNTs in which the number of shells are M and 2 respectively.

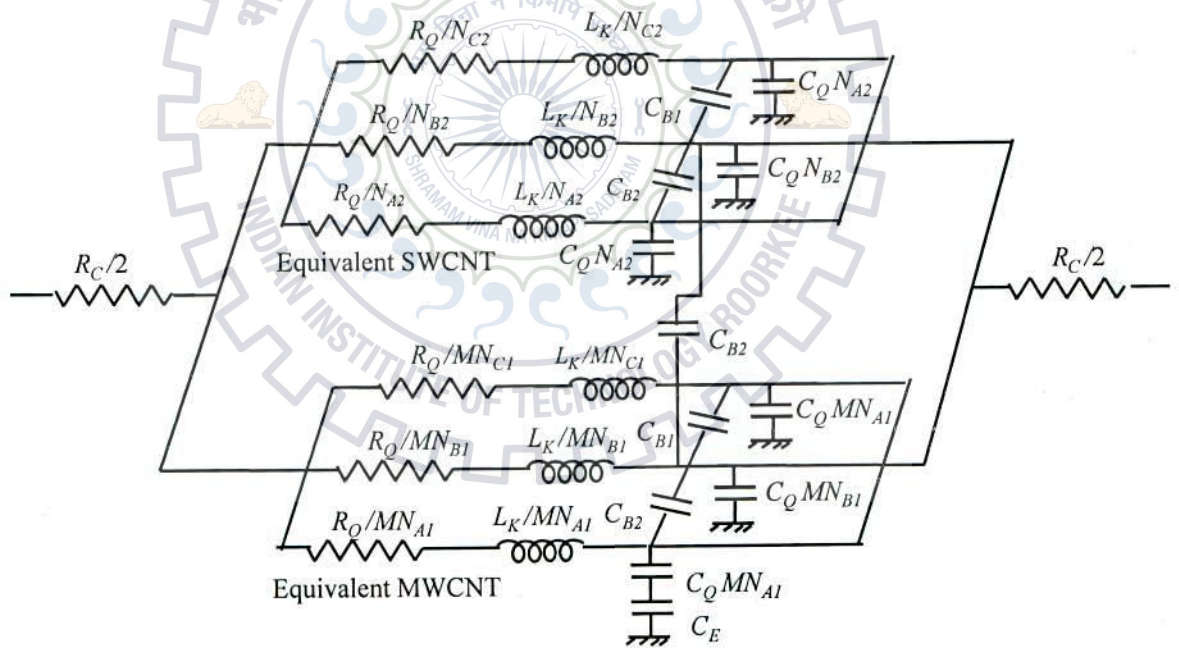


Figure 2.2 Equivalent RLC model of MCB

B. RLC Interconnect parasitic

The equivalent model of MCB consists of metal-nanotube contact resistance (R_C) at both ends which has a typical value of 0-100k Ω [7]. The quantum resistance (R_Q) in Fig. 2.2 is the

minimum resistance offered by quantum wire in ballistic region, *i.e.*, the region where there is no scattering along the quantum wire and can be expressed as [33]

$$R_Q = \frac{h}{4e^2} \approx 6.45k\Omega / \mu m \quad (8)$$

where e and h denotes charge of electron and Planck's constant respectively.

The equivalent RLC model of Fig. 2.2 comprises of kinetic inductance (L_K) that arises due to the kinetic energy of electrons and can be expressed as [33]

$$L_K = \frac{h}{2e^2 v_F} \quad (9)$$

where v_F denotes the Fermi velocity of CNT $\approx 8 \times 10^5$ m/s [10]. Due to the spin degeneracy in two conducting channels of SWCNT, the kinetic inductance of CNTs is defined as $L_K/4$ [33]

The outer shell of MWCNT offers electrostatic capacitances C_{ES} existing between the CNT and ground plane that can be expressed as [34]

$$C_{ES} = \frac{2\pi\epsilon}{\cosh^{-1}(2H/D)} \quad (10)$$

where H and D denotes the distance of MWCNT from ground plane and outermost shell diameter respectively. For $D = 1$ nm and $H = 1$ μ m the electrostatic capacitance C_{ES} is calculated to be approximately 50aF/ μ m [33]. Electrostatic capacitance C_{ES} is in series with C_Q , where C_Q is the quantum capacitance representing the finite density of states at the Fermi energy [33]. Apart from this, there is another capacitance known as coupling capacitance arises between the two CNTs or between the CNT bundles that can be expressed as follows [10]

$$C_Q = 2 \times \frac{2e^2}{h v_F} \quad (11)$$

$$C_B = \pi\epsilon l \left/ \ln \left[\left(\frac{d_{c-c}}{2r} \right) + \left(\sqrt{\left(\frac{d_{c-c}}{2r} \right)^2 + 1} \right) \right] \right. \quad (12)$$

where d_{c-c} , l , and r denotes the distance between the centre of any two CNTs, nanotube length and mean radius between two CNTs respectively. While considering a parallel layout of CNT interconnects, the C_B plays in a significant due to reducing feature size.

2.1.2 Model-II

This section demonstrates an equivalent single conductor (ESC) model of MWCNT, MWCNT bundle and MCB in which interconnect parasitic are evaluated using a square matrix of $M \times M$ dimensions where M is the number of CNTS in the Bundle. The elements of the matrix are interconnect parasitic such as capacitance, inductance and resistance. Using the approach of square matrix, equivalent parasitic such as quantum capacitance and intershell capacitance are modelled.

This approach can be applicable for both specific type and random type. In random type arrangement the position of each and every CNT must be known beforehand so that coupling capacitance can be modelled efficiently.

A. Proposed Equivalent Circuit Model

Using the concept of transmission line theory equivalent RLC modelling of MWCNT is carried out. RLC parameters have been evaluated for MWCNT and then the ESC model of MWCNT is extended to obtain the ESC model of MWCNT bundle and MCB. Different concentric shells in MWCNT are considered in parallel. The intershell capacitance between different shells is considered while modelling. This modelling considers a square matrix having M dimension wherein the matrix elements are considered as resistance, capacitance and inductance. This approach evaluates capacitive parasitic that considers coupling capacitance along with quantum capacitance and intershell capacitance.

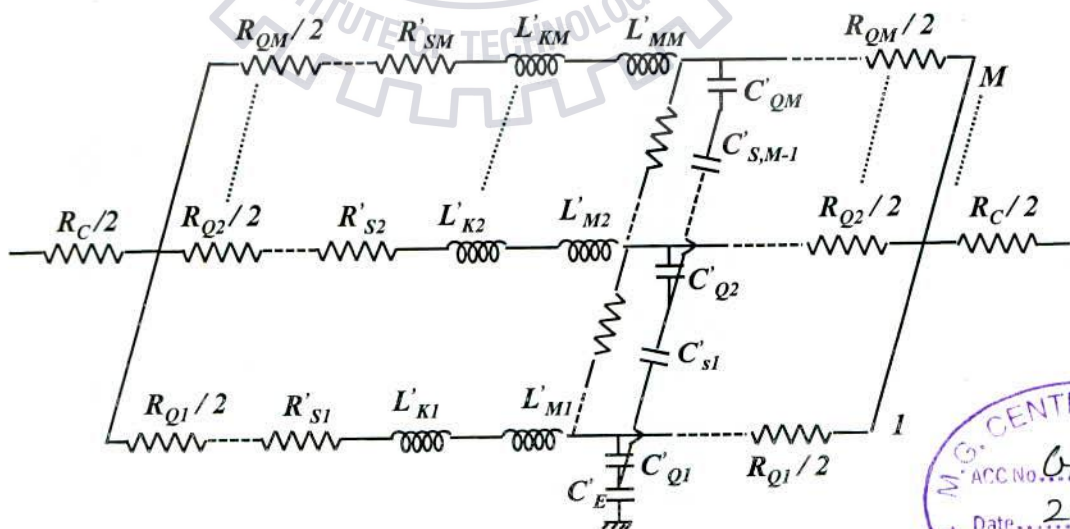


Figure 2.3 MTL model of distributed RLC network of MWCNT [7]



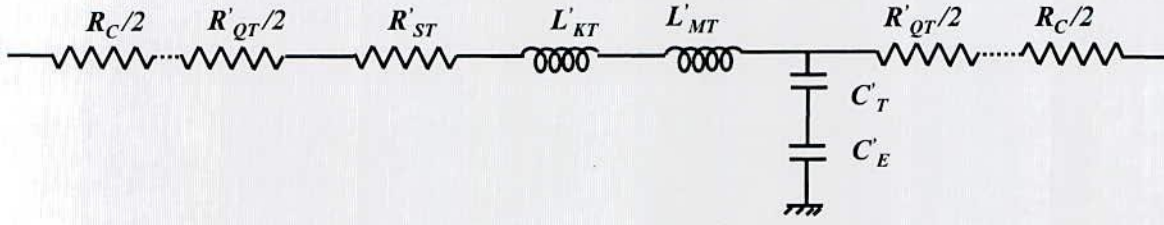


Figure 2.4 ESC distributed RLC circuit model of MWCNT

B. Interconnect parasitics of MWCNT

Interconnect parasitics are evaluated based on the total number of conducting channels in MWCNT. Conducting channels in MWCNT accounting the diameter dependency can be expressed as [9]

$$N_{shell} \approx 0.0612nm^{-1} \cdot D + 0.425, D > 3nm \quad (13)$$

where D denotes the diameter of any shell. Expression (13) introduces an error of 15% or less for diameter less than 3nm [9]. Fig. 2.4 presents the reference model given in [9], depending on the length, resistance can be categorized as: (1) Length independent resistance, it includes quantum/internal resistance (R_Q) and contact resistance, R_C (depends on fabrication process), (2) Length dependent resistance, it includes scattering induced resistance (R_S). Therefore, the resistance offered by i^{th} shell in MWCNT can be determined by

$$R'_{Ti} = R_{Qi} + R'_{Si} \cdot L = \frac{h}{2e^2 N_i} + \frac{h}{2e^2 N_i} \cdot \frac{L}{\lambda} \quad (14)$$

where R_{Qi} is considered as per expression (8) whereas L and λ represents the length of interconnect line and mean free paths respectively. For a particular shell (i.e., i), R'_{Ti} , R'_{Si} and R_{Qi} represents the resistance values whereas N_i is the number of conducting channels for that particular shell.

The MWCNT model shown in Fig. 2.4 comprises different inductance for different shell denoted by i : (1) kinetic Inductance (L'_{Ki}) that accounts the kinetic energy of electrons and (2) magnetic inductance (L'_{Mi}), which is primarily arises due to the magnetic field of MWCNT. Thus kinetic inductance for i^{th} shell can be expressed as [35]

$$L'_{K,i} = \frac{h}{2e^2 v_F N_i} \quad (15)$$

where v_F is the Fermi velocity of graphene and CNT which is equal to $8 \times 10^5 m/s$, L'_{ki} is the kinetic inductance for i^{th} shell.

In Fig. 2.4 two types of capacitances are considered: (1) quantum capacitance (C'_{Qi}) that accounts the density of electronic states in MWCNTs, (2) electrostatic capacitance (C'_E) as discussed in expression (10), (3) intershell coupling capacitance (C'_{Sij}), between two shells and (4) coupling capacitance (C'_C) between any two MWCNTs.

Fig. 2.5 presents the ESC model of the multi-line MWCNT model of Fig. 2.4. The interconnect parasitics of multi-line model discussed above are used to evaluate the interconnect parasitics of proposed ESC model using square matrix approach.

Using the approach of square matrix, the elements of capacitance can be modeled as

$$C'_{mat}(i, j) = \begin{cases} C'_{QM}, & \text{for } i = j \\ C'_{Sij}, & \text{for } i > j \\ C'_{Sji} = C'_{Sij}, & \text{for } j > i \end{cases} \quad (16)$$

In equation (16), C'_{QM} denotes the quantum capacitance as expressed in (11) on the other hand C'_{Sij} between i^{th} and j^{th} shell as expressed in (12). Therefore, the matrix can be represented as

$$C'_{mat} = \begin{bmatrix} C'_{Q1} & C'_{S12} & C'_{S13} & C'_{S14} \\ C'_{S21} & C'_{Q2} & C'_{S23} & C'_{S24} \\ C'_{S31} & C'_{S32} & C'_{Q3} & C'_{S34} \\ C'_{S41} & C'_{S42} & C'_{S43} & C'_{Q4} \end{bmatrix} \quad (17)$$

The quantum capacitance per shell can be further defined according to the number of conducting channels [9]

$$C'_{Qi} = C'_{Q/channel} \times N_i, \quad i \in 1 \text{ to } M \quad (18)$$

where N_i denotes the number of conducting channels of i^{th} shell and $C'_{Q/channel}$ is about 193aF/ μm [13].

The intershell coupling capacitance is expressed as

$$C'_{Sij} = \frac{2\pi\epsilon}{\ln\left(\frac{D_i}{D_j}\right)}, \quad \text{for } i > j \quad (19)$$

Using energy conservation approach and assuming that there is no current redistribution within the shells of MWCNT, the overall loop capacitance of MWCNT with its parallel ground return path can be defined as [35]

$$C'_{lp} = i_t^T \cdot C'_{mat} \cdot i_t^T \quad (20)$$

where i_t denotes the normalize current vector for each nanotube, C'_{mat} denotes the partial

capacitance matrix that considers intershell coupling capacitance and quantum capacitance. On the other hand, C'_{lp} is the $(M \times 1)$ matrix that denotes the equivalent capacitance for individual shell in column. In this approach it assumed that current is uniformly distributed in each shells of MWCNT. Thus, equivalent capacitance of the equivalent circuit is obtained as follows

$$C'_T = \sum_{i=1}^M C'_{lp}(i,1) \quad (21)$$

Apart from this, coupling capacitance and electrostatic capacitance can be obtained from expression (10) and (12) respectively.

In case of resistance modelling, R_{Qmat} is evaluated by considering the diagonal elements as quantum resistance and others as tunnelling conductance. Tunnelling conductance offers high resistive path and thus neglected. R'_{Qlp} , R'_{Slp} and L'_{Klp} can be evaluated similar to equation (17) and finally, the total resistance R'_{QT} and R'_{ST} and inductance L'_{KT} can be calculated as

$$R'_{QT} = \left(\sum_{i=1}^M (R'_{Qlp}(i,1))^{-1} \right)^{-1}, \quad R'_{ST} = \left(\sum_{i=1}^M (R'_{Slp}(i,1))^{-1} \right)^{-1} \quad \text{and} \quad L'_{KT} = \left(\sum_{i=1}^M (L'_{Klp}(i,1))^{-1} \right)^{-1} \quad (22)$$

C. Interconnect parasitics of MWCNT bundle

The ESC model obtained for MWCNT is extended to obtain the ESC model of MWCNT bundle, the only difference is that the interconnect parasitics are divided by the total number of nanotubes in the bundle which is calculated using expression (3- 4). MWCNT bundle requires parameters evaluated from ESC model of single MWCNT. MWCNT bundle contains many MWCNT which are replaced with their ESC model discussed in section 2-B. The constraints involved while using approach of MWCNT to derive MWCNT bundle are

1. Order of the square matrix depends on the total number of MWCNT in the bundle instead of total number of shells in MWCNT.
2. Diagonal elements are replaced by resistance/ capacitance/inductance obtained after ESC transformation whereas other elements are replaced with tunneling resistance/ coupling capacitance/mutual inductance between them respectively.

D. Interconnect parasitic for MCB

MCB can be modelled by approach discussed for MWCNT and MWCNT Bundle. In MCB shown in Fig. 2.6 there can be three types of coupling capacitance involved (1) C_{C1} coupling capacitance between two SWCNTs (2) C_{C2} coupling capacitance between SWCNT and

MWCNT, and (3) C_{C3} coupling capacitance between two MWCNTs. The value of these coupling capacitance can be calculated using equation (12). These all three coupling capacitances with quantum capacitance are used to form square capacitance matrix with the help of equation (16) to equation (21). In order to calculate the resistance square matrix, quantum resistance or scattering resistance with the tunnelling resistance is taken into account as per expression (22). Similarly, inductance square matrix can be evaluated by magnetic and kinetic inductance. RLC parameters are calculated by using equation (13) and equation (22).

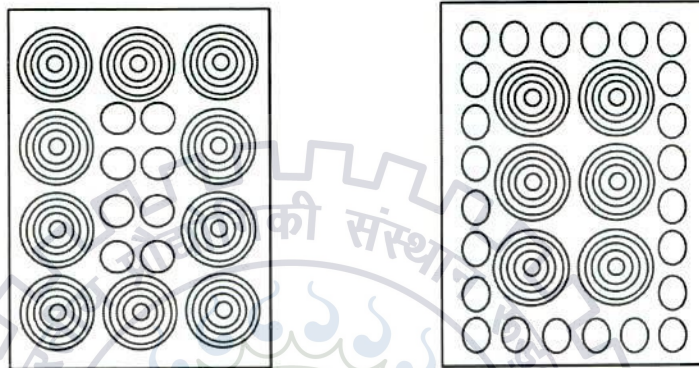


Figure 2.5 Figure showing MCB structure with (a) MWCNT in outer periphery and SWCNT filled inside and (b) SWCNT in outer periphery with MWCNT filled inside

2.2 RLC Circuit Modelling of Randomly Arranged MCB

This section provides a detailed description of the realistic MCB that follows the Gaussian distribution of CNTs in a bundle. Depending on the distribution and mean diameter of CNTs, an analytical model of MCB is presented.

2.2.1 Model-III

The geometry of SWCNT and MWCNT above ground plane is presented in Fig. 2.6. The diameter of SWCNT is referred as D whereas MWCNTs with large number of shells consists of innershell and outershell diameters of D_1 and D_n respectively. In current fabrication technology, the intershell spacing in MWCNT is equivalent to the Vander-waal's gap $\delta \approx 0.34\text{nm}$. If the outershell diameter of MWCNT is known, the number of shells p in a MWCNT can be obtained as [36]

$$p = 1 + \text{Inter} \left[\frac{D_n - D_1}{2\delta} \right] \quad (23)$$

The random distribution of CNTs having different diameters is shown in Fig. 2.1(c). MCB consists of J types of CNTs with different diameters wherein maximum and minimum diameters are considered as D_{max} and D_{min} respectively. Thus

$$D_{min} = [\bar{x} - 3.\sigma]; \quad D_{max} = D_{min} + 2.\delta.(J-1) \quad (24)$$

where

$$J = 3\sigma/\delta \quad (25)$$

D_{min} in expression (24) approximates to the value of discrete diameters as expressed in (23). Thus, the minimum and maximum number of shells P_{min} and P_{max} corresponds to D_{min} and D_{max} respectively that can be expressed as

$$P_{max} = P_{min} + J - 1 \quad (26)$$

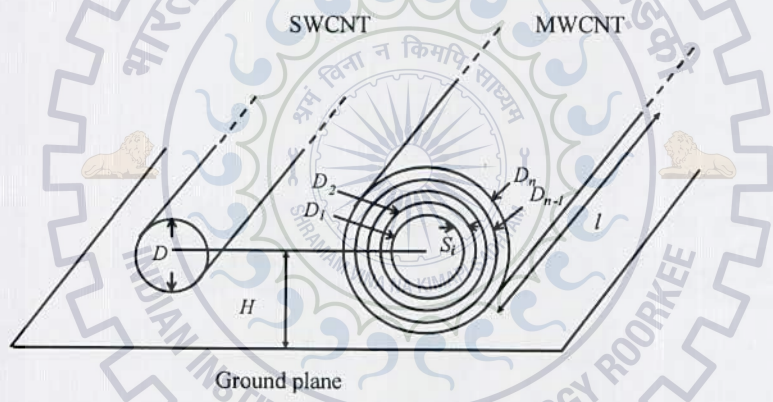


Figure 2.6 Geometry of SWCNT and MWCNT above ground plane

A. Gaussian distribution and probability theory

Depending on process control and techniques, CNT diameters inside the bundle follows Gaussian distribution [30] [37]. Using the analytical approach, the total number of CNTs in a bundle (N_{bundle}) can be obtained as [10]

$$N(D_{outer}) = \frac{N_{bundle}}{\sigma_{Douter} \sqrt{2\pi}} \exp \left[-\frac{1}{2} \left(\frac{D'_{outer} - \overline{D_{outer}}}{\sigma_{Douter}} \right)^2 \right] \quad (27)$$

where D'_{outers} , σ_{Douter} and $N(D_{outer})$ represents the mean diameter, standard deviation and number of tubes having outer diameter D_{outer} respectively. The graphical interpretation of (27)

is shown in Fig. 2.8(a) that indicates lesser numbers of CNTs having maximum and minimum diameters as compared to the CNTs with mean diameter.

Figure 2.8(b) demonstrates a polynomial relationship between the mean diameter and tube density as expressed in (28). The expression (28) suggests that for a given MCB having random distribution, more number of CNTs with smaller diameters can be accommodated as compared to the CNTs having larger diameters.

$$\text{Tube density} = A + B.D_{\text{mean}} + C(D_{\text{mean}})^2 + D.(D_{\text{mean}})^3 \quad (28)$$

where A , B , C and D have the constant values of 3.34705, -0.90728, 0.08827 and -0.00288 respectively.

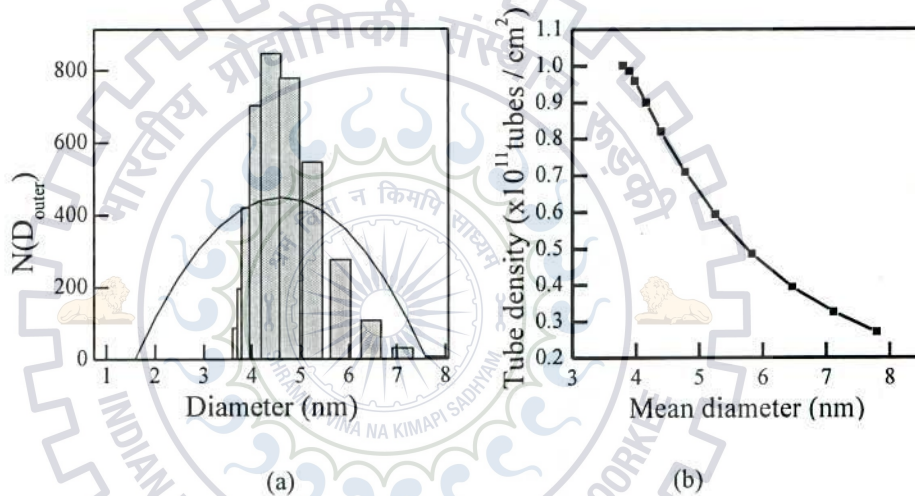


Figure 2.7(a) Tube density variation for different mean diameter of CNTs and (b) Gaussian distribution of CNTs having different mean diameters

If X is a diameter of a particular shell with mean \bar{x} and standard deviation σ , the probability of X being less than x_i is [38]

$$P(X < x_i) = \int_{-\infty}^{x_i} \left(\frac{1}{\sqrt{2\pi}} \exp\left(-\frac{1}{2}X^2\right) \right) dX \quad (29)$$

where x_i represents the outer shell diameter that can have values as (1), with an innershell diameter of 1nm and number of shells as p where $i \in 1, 2, 3 \dots p$.

Once cumulative probability is evaluated from (29), probability of the presence for a particular shell p_i having diameter d_i can be expressed as

$$P(X = x_i) = P(X < x_i) - P(X < x_{i+1}) \quad (30a)$$

$$P(D = d_i) = P(D < d_i) - P(D < d_{i+1}) \quad (30b)$$

Using the probability theory, expression (27) can be minimized for total number of CNTs in bundle that exhibits the probability of a particular outer diameter in MCB as

$$N(D_{outer}) = N_{bundle} \times P(D = D_{outer}) \quad (31)$$

Table I presents the number of CNTs of a particular outer diameter for different bundle densities ranging from 10^9 to 10^{12} tubes/cm² as calculated from (27) to (31). For an instance, a MCB having fixed bundle area, mean diameter and standard deviation of $4\mu\text{m}^2$, 4.2nm and 1.25nm [30] respectively, a total number of 3999 CNTs can exist as observed from Table 2.1.

In current fabrication process, the diameter of SWCNTs is upto tens of nanometers. This research work considers a finite probability that CNTs having D_{outer} can be either SWCNT or MWCNT. So as to analyze the effect of diameter of SWCNTs in MCB, a new variable D_R is introduced. The variable D_R can have the diameter ranging from

$$D_{min} \leq D_R \leq D_{max} \quad (32)$$

The quantitative value of D_R assumes that CNTs having diameter $\leq D_R$ can be considered as SWCNTs, while the CNTs with diameters $> D_R$ are referred as MWCNTs. For an instance, MCB with a fixed bundle area of $4\mu\text{m}^2$ has $J = 11$ for which D_{min} and D_{max} are calculated as 1nm and 7.8nm respectively as presented in Table II. Subsequently, P_{min} and P_{max} corresponds to the values of 1 and 11 respectively that exhibits the D_R ranging from 1nm to 7.8nm.

B. RLC Interconnect model

This section presents an exact multi-conductor transmission line (MTL) formulation [39] that replicates the behaviour of MCB. The interconnect parasitics of the MTL model primarily depends on the total number of conducting channels associated with each type of CNT in a bundle. Number of conducting channels for a particular shell in MWCNT (or particular diameter of SWCNT) is determined using the number of sub-bands crossing at Fermi level. Thus, the total number of conducting channels (N_{total}) of CNTs is the function of Fermi Dirac distribution and can be approximated as per expression (13)

Modelling of the interconnect parasitics is carried out based on the CNTs having different types as expressed in (25). Thus, the MTL model of MCB is presented in Fig. 2.9 that considers n_j and N_j denoting the number of CNTs and corresponding number of conducting channels of J^{th} type respectively. The number of conducting channels associated with each

type of CNT is used to model the interconnect parasitics. The equivalent model of Fig. 2.9 is simplified assuming that all CNTs in an MCB are connected in parallel and connected at both ends with same potential across each transmission line. Under this consideration, Fig. 2.10 finally presents a simplified equivalent single conductor (ESC) model of MCB.

Table 2.1 Diameters and Corresponding number of CNTs for different Bundle density

Diameter (nm)	Number of CNTs (n_i) for different bundle density (tubes / cm^2)			
	10^9	10^{10}	10^{11}	10^{12}
1.00	1	9	87	868
1.68	2	20	196	1964
2.36	4	42	422	4216
3.04	7	70	703	7032
4.40	8	85	846	8464
3.72	8	78	778	7776
5.08	5	55	546	5456
5.76	3	27	275	2748
6.44	1	11	108	1084
7.12	0	3	30	304
7.80	0	1	7	68

Table 2.2 Numbers and Corresponding Diameters of SWCNTs and MWCNTs in a MCB (Bundle Area= $4\mu\text{m}^2$) for Different Values of D_R

D_R (nm)	Numbers of SWCNTs with diameter $\leq D_R$	Numbers of MWCNTs with diameter $> D_R$
1.00	87	3912
1.68	283	3716
2.36	705	3294
3.06	1408	2591
3.72	2254	1745
4.40	3032	967
5.08	3578	421
5.76	3854	145
6.44	3962	37
7.12	3992	7
7.80	3999	0

Table 2.3 Diameters and Corresponding number of CNTs for different Bundle density

Diameter (nm)	Number of CNTs (n_j) for different bundle density (tubes / cm ²)			
	10 ⁹	10 ¹⁰	10 ¹¹	10 ¹²
1.00	1	9	87	868
1.68	2	20	196	1964
2.36	4	42	422	4216
3.04	7	70	703	7032
4.40	8	85	846	8464
3.72	8	78	778	7776
5.08	5	55	546	5456
5.76	3	27	275	2748
6.44	1	11	108	1084
7.12	0	3	30	304
7.80	0	1	7	68

Table 2.4 Numbers and Corresponding Diameters of Swcnts and Mwcnts in a MCB (Bundle Area=4μm²) for Different Values of D_r

D_R (nm)	Numbers of SWCNTs with diameter $\leq D_R$	Numbers of MWCNTs with diameter $> D_R$
1.00	87	3912
1.68	283	3716
2.36	705	3294
3.06	1408	2591
3.72	2254	1745
4.40	3032	967
5.08	3578	421
5.76	3854	145
6.44	3962	37
7.12	3992	7
7.80	3999	0

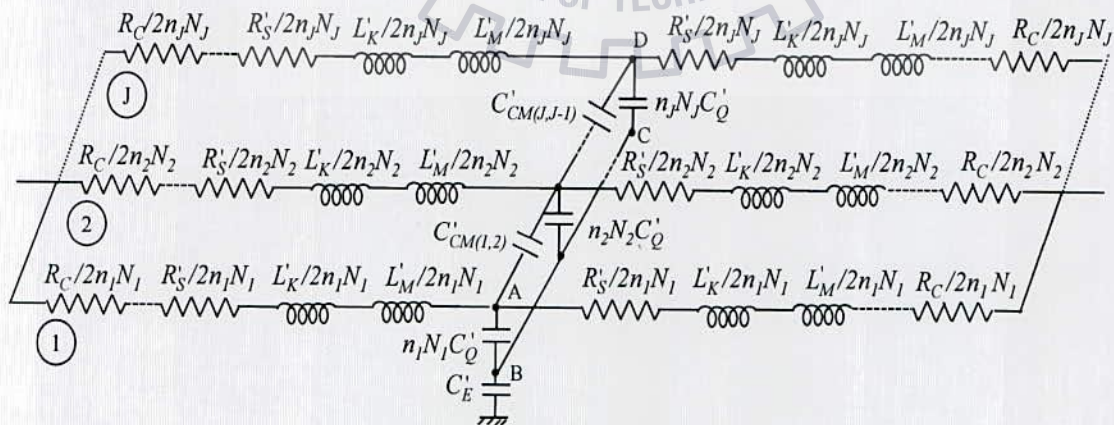


Figure 2.8 MTL model of MCB

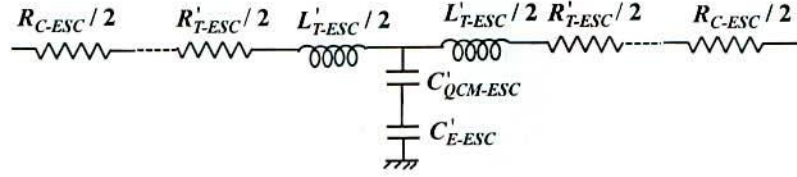


Figure 2.9 ESC model of MCB

C. Interconnect Parasitics

The ESC model of Fig. 2.10 consists of contact resistance (R_{C-ESC}), quantum resistance (R_{Q-ESC}) and scattering resistance (R_{S-ESC}) as per expression (8) that are derived from contact resistance (R_C), scattering resistance (R_S) and quantum resistance (R_Q) similarly. However, the ESC model of Fig. 5 also considers the scattering resistance (R_{S-ESC}). Therefore, the R_{C-ESC} and the *p.u.l.* R'_{ESC} can be expressed as

$$R_{C-ESC} = \left(\sum_{i=1}^J \left(\frac{R_C}{2nJNJ} \right)^{-1} \right)^{-1} \quad \text{and} \quad R'_{S-ESC} = \left(\sum_{i=1}^J \left(\frac{R_Q}{\lambda nJNJ} \right)^{-1} \right)^{-1} \quad (33a)$$

where

$$R_{Q-ESC} = \left(\sum_{i=1}^J \left(\frac{h}{2e^2 nJNJ} \right)^{-1} \right)^{-1} \quad (33b)$$

where h , e , λ , L and N denotes the Planck's constant, charge of electron, mean free path, interconnect length and total number of conducting channels respectively.

The MTL model of Fig. 2.9 accounts for two types of inductances: (a) kinetic inductance (L_K) and (b) magnetic inductance (L_M). Therefore, the total inductance of MCB in Fig. 2.10 can be expressed as [7]

$$L'_{ESC} = L'_{K-ESC} + L'_{M-ESC} \quad (34)$$

where

$$L'_{K-ESC} = \left(\sum_{i=1}^J \left(\frac{h}{2e^2 v_F nJNJ} \right)^{-1} \right)^{-1} \quad (35)$$

and

$$L'_{M-ESC} = \frac{\mu}{2\pi} \cosh^{-1}(2H/D_{outer}) \quad (36)$$

CNTs in a bundle facing the ground (N_B) experiences an electrostatic capacitance (C_{E-ESC}) that arises due to the change in electrostatic potential. Therefore, the *p.u.l.* electrostatic capacitance (C'_{ESC}) can be obtained as

$$C'_{E-ESC} = \frac{2\pi\epsilon}{\cosh^{-1}(2H/D_{outer})} \cdot N_B \quad (37)$$



3 Performance Analysis

In this chapter, propagation delay, power dissipation and crosstalk delay are analyzed for MCB having different arrangements of CNTs. Model-I and Model-II are used to analyze the bundle having specific arrangements whereas Model-III is used for MCB having Gaussian distribution of CNTs inside it. Coupling of energy with nearby interconnect is the primary reason of crosstalk interference and is classified as dynamic and functional crosstalk. In case of dynamic crosstalk, the noise arises due to the simultaneous switching of signals in adjacent interconnect lines either in opposite or in same phase. Opposite switching cause the maximum noise and regarded as worst case scenario. On the other hand, functional crosstalk relates to the voltage spikes that arises in the quiet interconnect line due to switching of signal in aggressor interconnect line. This chapter only considers the effect of dynamic crosstalk.

3.1 Simulation Setup

In order to analyze the propagation delay, power dissipation and crosstalk at different interconnect lengths a driver-interconnect-load (DIL) system is used. HSPICE simulator is used for simulating the *RLC* model of interconnect line. CMOS inverter is used to drive the *RLC* equivalent of CNT bundle interconnect having a capacitive load at output. In simulation setup a CMOS inverter at 32nm technology node is used [40] for which the technology parameters for NMOS are 32nm and 640nm and for PMOS are 32nm and 1280nm considered for bundle height and width, respectively. As shown in Fig. 3.1, the input is triggered at 50% of supply voltage whereas the output fall time is target at 50%. The delay and power dissipation is analyzed for different bundle structures of MCB.

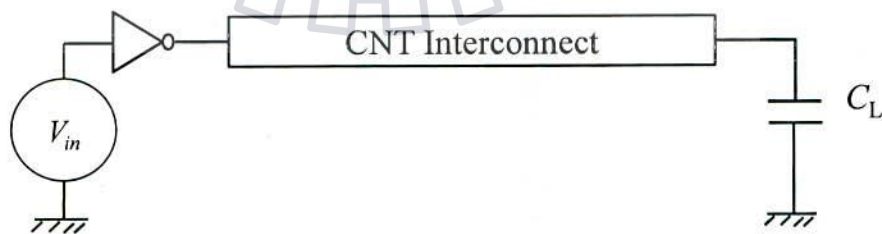


Figure 3.1 Simulation setup for MWCNT interconnects with CMOS inverter used as driver

Simulation Setup for 2-line Bus Architecture

Crosstalk delay is analysed using 2-line bus architecture as shown in Figure 3.2. Out of these two, one is denotes the aggressors and other as victim. The interconnect line can be replaced

by *RLC* model of any of CNT interconnect model discussed in previous chapter. The bus architecture model has the load capacitance (C_L) and power supply voltage (V_{dd}) as 10aF and 1V respectively. HSPICE simulations have been performed where aggressor and victim lines are switching simultaneously in opposite direction (dynamic crosstalk). Crosstalk delay is analysed at different local and global lengths. The coupling capacitance (C_{CM}) considered between two MCB interconnect can be evaluated using expression (12)

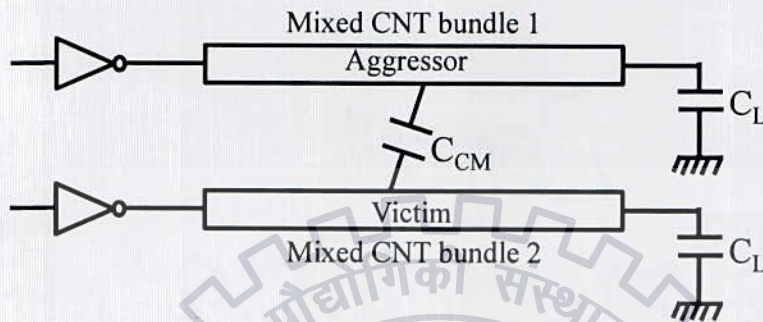


Figure 3.2 Two-line bus architecture of CNTs [21]

3.2 Crosstalk and Power dissipation Analysis using Model-I

Using the mentioned set up in section 3.1 and equivalent RLC model discussed in section 2.1.1, crosstalk delay and power dissipation are observed for different bundled CNT structures. The bundle interconnect analysed using Model-I are bundled SWCNT, bundled DWCNT, MCB-I, MCB-II that are shown in Figure 2.1(a), 2.1(b), 2.1(d) and 2.1(e) respectively. For different interconnect lengths, Figs. 3.3 and 3.4 represents crosstalk delay and power dissipation respectively. Both the performances are significantly improved for MCB-II in comparison to MCB-I, bundled SWCNT and bundled DWCNT interconnects. This is primarily due to their structural differences.

Using the MCB-II structure, percentage improvement is observed for crosstalk delay that is summarized in Table 3.2. It is observed that on an average, crosstalk delay of MCB-II is improved by 86.01% as compared to bundled SWCNT. The reason behind is the unique geometry of MCB-II that contains MWCNTs and SWCNTs in equal halves within the bundle. The primary benefit of this structure is the fact that the outermost shell of MWCNTs carries lower current as compared to a SWCNT or DWCNT due to the effect of fractional conductance observed in MWCNTs [10]. Sanvito et al. [41] reported that the outermost shell of MWCNT exhibits to have fractional conductance i.e., non-integer quantum conductance values that arises due to the interaction between the walls. This interaction can cause blocking

of some quantum conductance channels and redistribution of the current non-uniformly over individual shells within the MWCNT [41]. As a result, the outermost shells of MWCNTs shield the inner shells. Therefore, the effect of crosstalk delay becomes less for MCB-II as compared to other bundled CNT structures

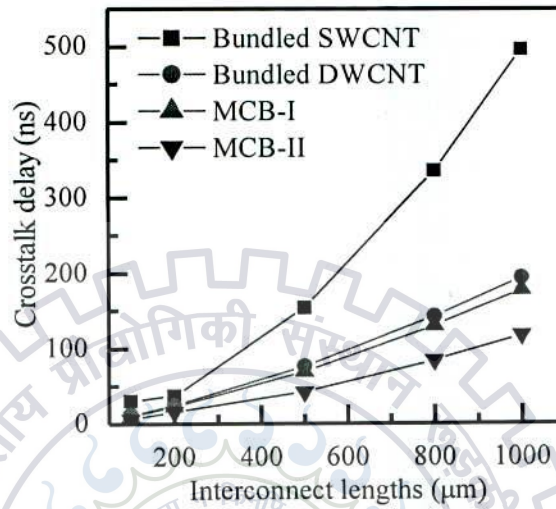


Figure 3.3 Crosstalk for different interconnect lengths for different bundled CNT structures

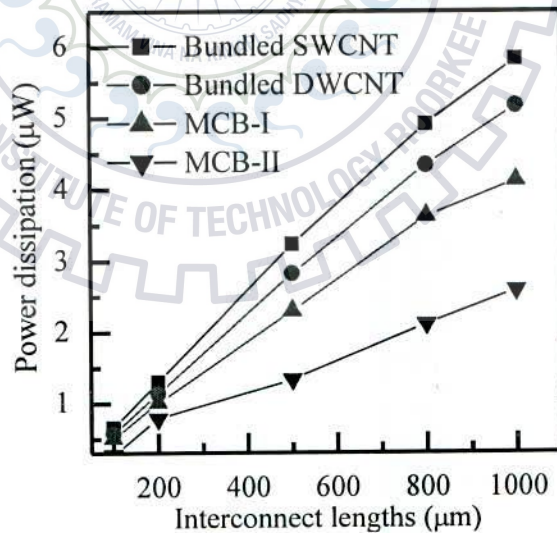


Figure 3.4 Power dissipations for different bundle structure at different lengths

Table 3.1 Improvement in Crosstalk for MCB-II w.r.t. Other bundled CNT structures

Interconnect lengths (μm)	Percentage improvement in MCB-II with respect to		
	Bundled SWCNT	Bundled MWCNT	MCB-I
100	81.78	52.13	46.53
200	84.42	56.71	49.74
500	86.52	59.53	50.38
800	87.99	61.00	51.35
1000	89.36	63.39	54.01

Table 3.2 Percentage improvement in power dissipation for MCB-II w.r.t. other bundled CNT structures

Interconnect lengths (μm)	% improvement in MCB-II with respect to		
	Bundled SWCNT	Bundled MWCNT	MCB-I
100	58.24	52.08	45.62
200	59.66	53.31	47.21
500	60.60	54.82	51.41
800	62.86	56.51	52.42
1000	62.56	59.88	57.10

Table 3.3 Equivalent interconnect parasitic for different Bundled CNT Structures

Interconnect parasitic	Bundled SWCNT	Bundled DWCNT	MCB-I	MCB-II
R_Q (Ω)	2.86	2.74	1.51	1.08
L_K (pH)	17.88	7.59	1.01	0.27
C_Q (fF)	48.01	33.88	14.28	2.89
C_E (fF)	0.94	0.14	0.14	0.03

Discussion

Percentage improvement in power dissipation using MCB-II is summarized in Table 3.3. The overall improvement in power performances is 61.33% more as compared to bundled SWCNT structure. The reason behind is their different interconnect parasitic. The quantitative values of parasitic primarily depend on bundle geometry and number of CNTs in bundle. The parasitic associated with different CNT bundles are placed in Table 3.4. As far as

the number of SWCNTs, DWCNTs and MWCNTs increases, the equivalent resistive and inductive parasitic reduces. This reduction is more for MWCNTs as compared to SWCNTs and DWCNTs due to a large number of shells. From Table 3.4, it can be illustrated that the equivalent parasitic reduces due to the presence of MWCNTs in MCB-II. Therefore, MCB-II results in least power dissipation as compared to MCB-I, bundled SWCNT and bundled DWCNT structures.

3.3 Propagation delay Analysis using Model-II

This section illustrates propagation delay for single, bundled MWCNT and different mixed CNT bundle structures at global VLSI interconnects.

3.3.1 MWCNT

This section proposes a novel ESC model (Model-II) for MWCNT interconnects. So as to verify the model, it is compared with the model proposed by Li *et al* [9]. Using the reference model [9] and novel model, HSPICE simulations have been performed to analyze the propagation delay for different number of shells such as 5, 10 and 15 and for various lengths ranging from 100 μm to 1000 μm . The results of propagation delays are summarized in Table 3.5. It is observed that the novel ESC model estimates propagation delay with an error of 1.67% or less as compared to the reference one [9]. The key advantage of this proposed model is that the percentage error in delay for the novel ESC model is reduced for increasing interconnects lengths and number of shells in MWCNT.

3.3.2 MWCNT Bundle

Using the novel modelling approach, propagation delay is compared for different MWCNT bundle with area of (12 \times 24) nm^2 , (28 \times 56) nm^2 and (44 \times 90) nm^2 . The propagation delay is evaluated for varying interconnects lengths ranging from 100 μm to 1000 μm . The variations of delay with different bundle dimensions are summarized in Table 3.5. It is observed that the overall improvement in delays are 68.52% and 27.34% for bundle area of (44 \times 90) nm^2 as compared to the bundle areas of (12 \times 24) nm^2 and (28 \times 56) nm^2 respectively. The reason behind is the number of MWCNTs in bundle that increases for larger bundle areas. Propagation delay primarily depends on resistive and capacitive parasitic that reduces with increasing number of MWCNTs in bundle. Therefore, MWCNT with larger bundle area has significant improvement in delay as compared to the smaller one.

Fig. 3.5 depicts the variation in propagation delay with interconnect lengths for different number of shells in MWCNT bundle. It is observed that for a specific bundle area, propagation delay reduces for higher number of shells in MWCNT at global interconnect lengths. The reason behind is that the number of conducting channels that are directly proportional to the number of shells. With more number of conducting channels associated, MWCNT bundle with 15 shells results in least propagation delay as compared to bundled MWCNTs with 5 and 10 shells.

Table 3.4 Comparison of propagation delay between reference model [9] and proposed esc model

Interconnect Length	No. of Shells	Propagation delay (in ns)		% error introduced in ESC w.r.t. multiline model
		Multi-Line model [9]	ESC Model	
100 μ m	5	0.68	0.69	3.51
	10	0.32	0.32	2.83
	15	0.19	0.19	2.44
500 μ m	5	9.76	10.07	3.2
	10	4.69	4.82	2.67
	15	2.94	3.01	2.40
1000 μ m	5	358.51	371.09	1.88
	10	173.97	178.89	1.64
	15	10.952	11.219	1.47

Table 3.5 Propagation Delay for Different MWCNT Bundle Areas at Global Interconnect Lengths

Interconnect Length	No. of shells used in bundle	Percentage improvement in delay for (44x90 nm ²) w.r.t other bundle area such as	
		12x24 nm ²	28x56nm ²
100	5	52.86	6.15
	10	58.80	13.78
	15	60.41	14.98
500	5	73.26	32.01
	10	73.53	32.47
	15	73.63	35.94
1000	5	74.54	36.02
	10	75.36	36.37
	15	75.54	39.12

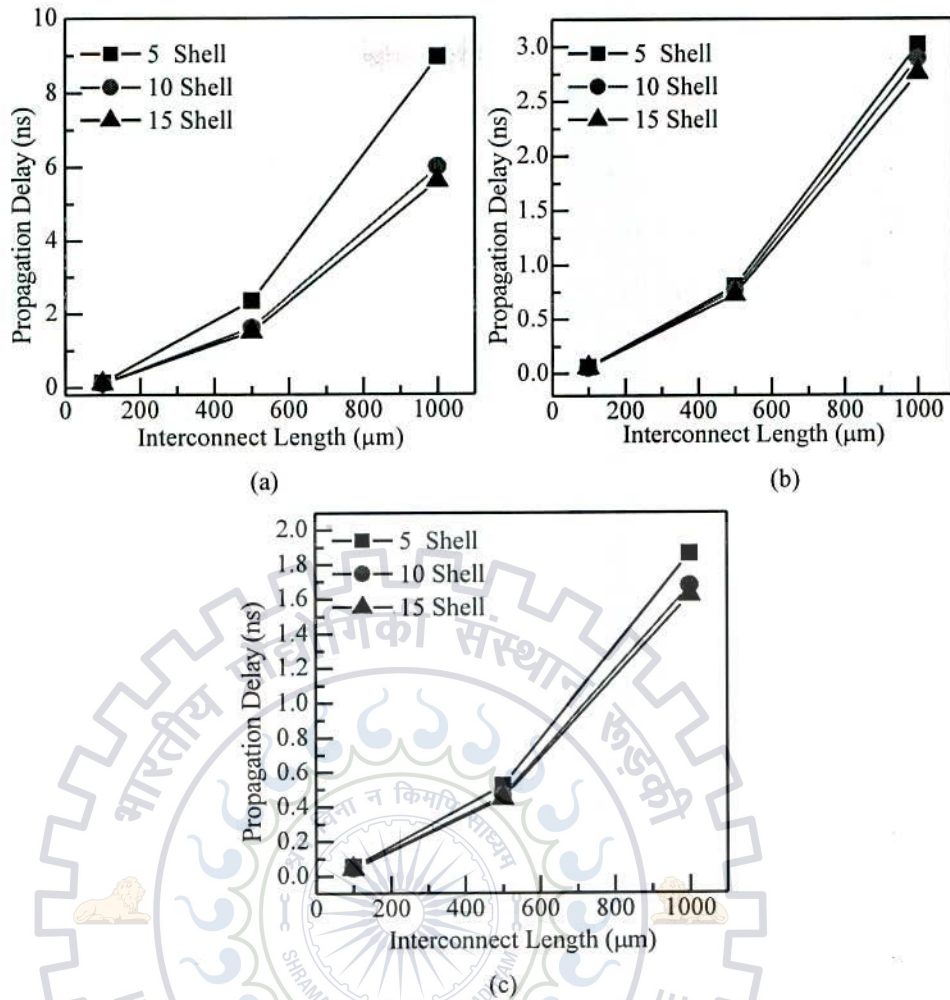


Figure 3.5 Propagation delay with varying interconnect lengths for bundled MWCNT that has the area of (a) $12 \times 24 \text{ nm}^2$ (b) $28 \times 56 \text{ nm}^2$, & (c) $44 \times 90 \text{ nm}^2$.

3.3.3 MCB

Modelling approach discussed in section 2.2.1 is implemented to MCB structure shown in Fig. 3.6. MCB-III consists of MWCNT as outer periphery and SWCNT inside whereas MCB-IV consists of SWCNT and MWCNT inside [10].

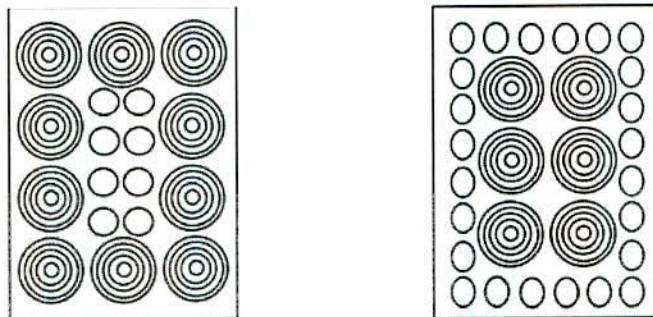


Figure 3.6 CNT Bundle showing (a) MCB-III and (b) MCB-IV [8]

Propagation delay of both MCB-III and MCB-IV is evaluated and given in Table 3.7. From the results it can be readily judged that MCB-III shows greater improvement in propagation delay over MCB-IV with average improvement of 64.7%. It is due to the fact that in case of MCB-III MWCNTs at outer periphery shields the inner CNTs more effectively as compared to MCB-IV having SWCNTs at outer periphery and MWCNTs inside [10].

Table 3.6 Propagation delay (in ns) for different interconnect length.

Length	Propagation Delay of MCB-III (in ns)	Propagation Delay of MCB-IV (in ns)	Percentage improvement in propagation delay of MCB-III over MCB-IV
100 μm	0.07	0.17	58.22
200 μm	0.21	0.59	65.112
500 μm	1.11	3.30	66.32
800 μm	2.73	8.27	67.05
1000 μm	4.21	12.85	67.27

Fig. 3.7 shows the propagation delay variation of MCB-III and MCB-IV over wide range of interconnect lengths. It has been observed that propagation delay of MCB-IV rises much faster as compared to MCB-III for increasing interconnect length. This can be understood by the fact that *p.u.l* interconnect parasitics of MCB-III are lower as compared to MCB-IV due to higher number of conducting channels. This deviation in interconnect parasitics increases as length increases.

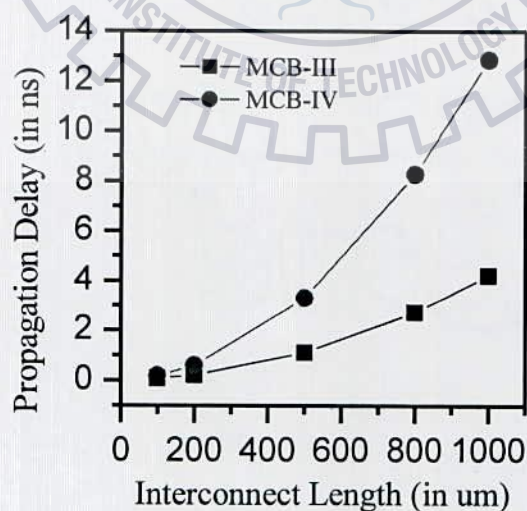


Figure 3.7 Propagation delay variation of MCB-III and MCB-IV for various interconnect length

Discussion

Model-II is used to analyse propagation delay performance of MCB-III and MCB-IV in which MCB-III has improvement in delay performance of 63.2% as compared to MCB-IV. It has been observed that for MWCNT bundle the overall improvement in propagation delay is 68.52% and 27.34% respectively for bundle dimension $44 \times 90 \text{nm}^2$ as compared to $28 \times 56 \text{nm}^2$ and $12 \times 24 \text{nm}^2$ respectively

3.4 Propagation, Power dissipation and Crosstalk delay Analysis using Model-III

This section provides a detailed insight of transient analysis for MTL and ESC models. Using the ESC model, different interconnect performance such as propagation delay, power dissipation and crosstalk are also analysed for MCBs.

3.4.1 Transient Analysis of MTL and ESC

Transient analysis is performed for the exact MTL (Fig. 2.8) and the reduced ESC (Fig. 2.9) models of randomly distributed MCBs having a fixed bundle area of $(2 \mu\text{m} \times 2 \mu\text{m})$. The output voltage waveforms of both the MTL and ESC models are compared for an applied pulsed input having amplitude of 1 volt and an equal rise and fall time of 5 ps. The results are shown in Fig. 3.8 for 10, 50, 100 and $400 \mu\text{m}$ interconnect lengths. It is observed that the output voltage of the reduced ESC model is in good agreement with the exact MTL one at smaller interconnect lengths. However, at higher interconnect lengths, using both the MTL and ESC models, the deviation in output voltage waveforms increases and attains a maximum value of 71 mV at $400 \mu\text{m}$ interconnect length. Table 3.8 summarizes the propagation delay of the MTL and ESC model (τ_{MTL} and τ_{ESC}) at different interconnect lengths. It is observed that the deviation between τ_{ESC} and τ_{MTL} is negligible at 10, 50 and $100 \mu\text{m}$ interconnect lengths whereas at $400 \mu\text{m}$ interconnect length, the maximum deviation is 9.25% as compared to the MTL formulation.

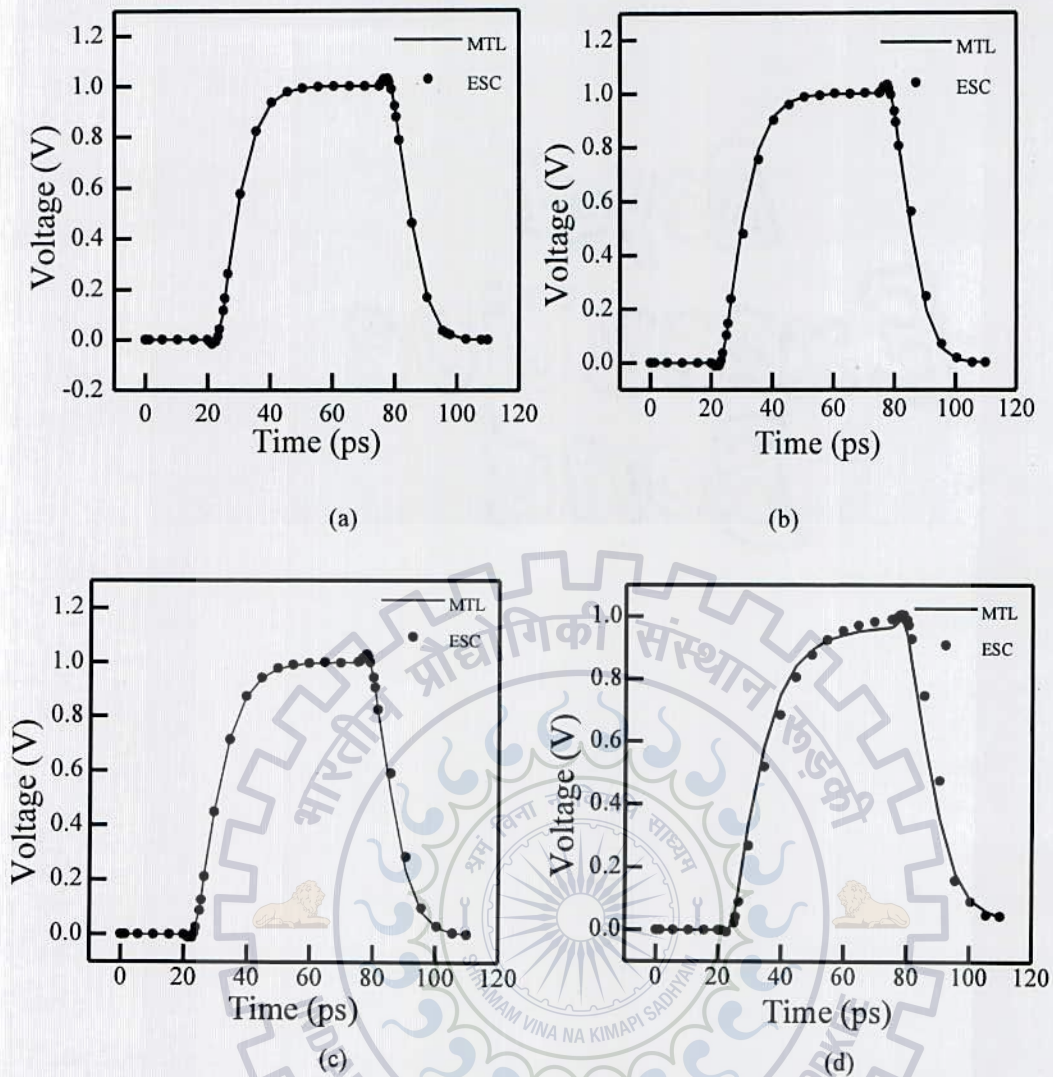


Figure 3.8 Output voltage waveforms at different interconnect lengths of (a) $10\mu\text{m}$, (b) $50\mu\text{m}$, (c) $100\mu\text{m}$ and (d) $400\mu\text{m}$, computed by means of an exact MTL formulation and a reduced ESC approach

Table 3.7 Propagation delays at Different interconnect lengths

Interconnect Lengths (μm)	10	50	100	400
τ_{MTL} (ps)	7.0296	7.3678	7.9911	10.549
τ_{ESC} (ps)	7.0308	7.3866	8.0049	11.625

3.4.2 Propagation delay and power dissipation

Propagation delay and power dissipation primarily depends on the interconnect parasitics that are calculated using the number of conducting channels associated with each CNT in a bundle as shown in Table 3.8. Fig. 3.9(a) shows the variation of propagation delay for different tube density as presented in Table 2.1. It is observed that the delay is significantly improves for higher tube density in a bundle. The primary reason is the higher number of conducting channels that increases with number of CNTs in a MCB. Apart from this, the variation of propagation delay for different D_R is shown in Fig. 3.9(b). As seen in Table 2.2, for higher value of D_R , the number of SWCNTs in a MCB increases while the number of MWCNTs reduces. Thus, the total number of conducting channels in a bundle reduces that effectively increases the delay for higher value of D_R .

Table 3.8 Interconnect Parasitics for Different Bundle Density

Interconnect parasitic	Interconnect parasitics for different bundle density (tubes/cm ²)			
	10 ⁹	10 ¹⁰	10 ¹¹	10 ¹²
N_{total}	133	1330	13723	138710
R_{S-ESC} ($\Omega/\mu\text{m}$)	97	9	0.94	0.093
L_{K-ESC} (pH/ μm)	60.2	5.76	0.58	0.05
L_{M-ESC} (fH/ μm)	200	18.7	1.8	0.18
C_{Q-ESC} (pF/ μm)	0.025	0.26	2.66	26.62
C_{E-ESC} (fF/ μm)	0.089	0.95	9.47	94.70

The tube count is primarily decided using the mean diameters of CNTs which are varied from 3.8nm to 7.8nm. Thus, it is desirable to reduce the mean diameter to accommodate more number of CNTs in a bundle as presented in Table 3.9. Fig. 3.10 exhibits the delay and power performance for different number of tubes in an MCB. For higher number of CNTs, propagation delay is considerably reduced with a negligible increment in power dissipation. As seen in Table 3.7, for higher tube density, resistive and inductive parasitics reduces whereas capacitive parasitic increases. Propagation delay primarily depends on the resistive and capacitive parasitics while the power dissipation is mainly governed by the capacitive one. At different interconnect lengths, resistive parasitic has dominating effect on capacitance that significantly reduces the overall delay. However, due to the increase in capacitance, a negligible increment in power dissipation is observed.

Table 3.9 Variation of Mean Diameter for Realistic MCB with a Fixed Bundle area of $4\mu\text{m}^2$

Diameter (nm)	Number of CNTs in MCB											
1.00	87	0	0	0	0	0	0	0	0	0	0	0
1.68	196	227	0	0	0	0	0	0	0	0	0	0
2.36	422	422	537	0	0	0	0	0	0	0	0	0
3.04	703	703	703	1004	0	0	0	0	0	0	0	0
3.72	846	846	846	846	1535	0	0	0	0	0	0	0
4.40	778	778	778	778	778	1872	0	0	0	0	0	0
5.08	546	546	546	546	546	546	1953	0	0	0	0	0
5.76	276	276	276	276	276	276	276	1793	0	0	0	0
6.44	108	108	108	108	108	108	108	108	1543	0	0	0
7.12	30	30	30	30	30	30	30	30	30	1292	0	0
7.80	7	7	7	7	7	7	7	7	7	7	7	1084
Mean diameter (nm)	3.80	3.90	3.99	4.16	4.40	4.78	5.25	5.83	6.46	7.12	7.80	

3.4.3 Crosstalk

This sub-section demonstrates the worst case crosstalk delay for out-phase switching scenario in capacitively coupled interconnect lines as presented in Fig. 3.2. The interconnect lines are represented by the ESC model of RLC as shown in Fig. 2.9.

Figure 3.11 exhibits the variation in crosstalk delay for different bundle density ranging from 10^9 to 10^{12} tubes/cm². It is observed that the crosstalk delay is significantly reduced for higher tube density in a bundle. The primary reason behind this reduced effect is the higher number of conducting channels that depends on the diameter and number of CNTs in an MCB [39] [9]. The higher number of conducting channels effectively reduces the equivalent resistive and inductive parasitics whereas capacitive parasitic is increased as presented in Table 3.7. This combined resistive and capacitive effect considerably reduces the propagation delay under the influence of dynamic crosstalk. Thus, the MCB having higher tube density exhibits reduced crosstalk delay at different interconnect lengths.

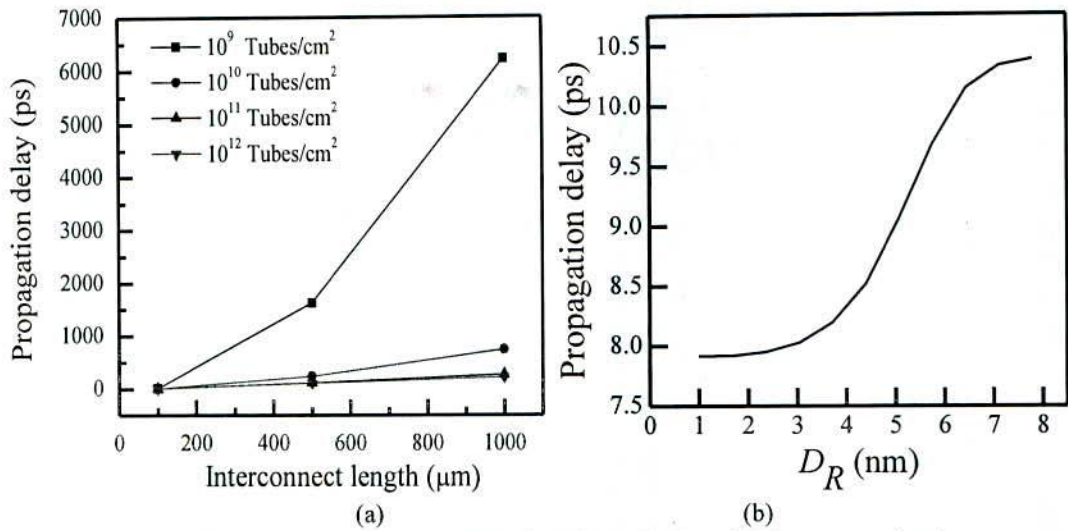


Figure 3.9 Propagation delay variation for different (a) D_R and (b) interconnect lengths

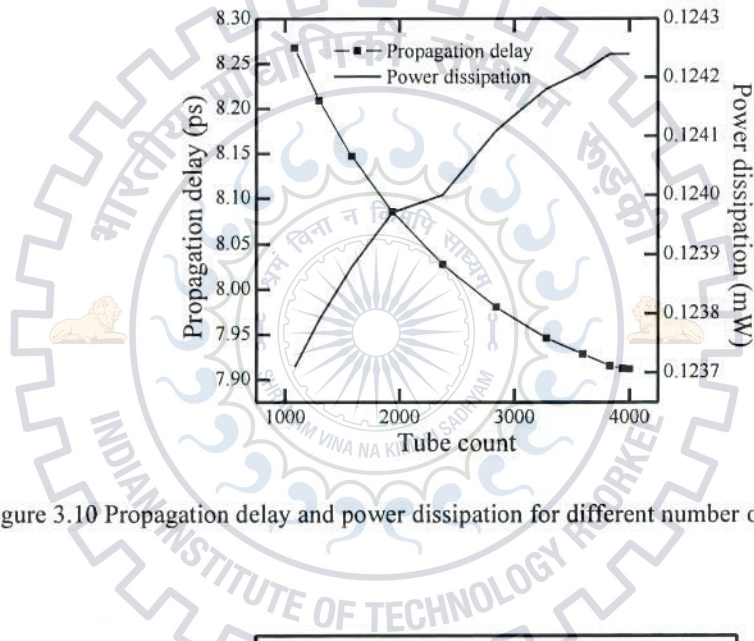


Figure 3.10 Propagation delay and power dissipation for different number of tubes in a MCB

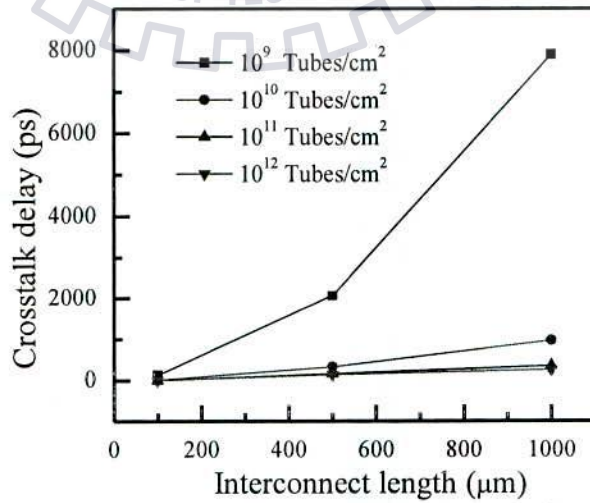


Figure 3.11 Crosstalk delays for different tube density in a MCB

4 Process variation in MCB

CNT bundle may consist of pure SWCNTs and pure MWCNTs or mixture of CNTs having different diameters. Due to less complexity involved in fabrication, MCB is preferred wherein SWCNTs, DWCNTs and MWCNTs are randomly arranged [30]. MCB is the natural bundle available post fabrication. Advancement in technology results in shrinking of device dimension that causes densely packed ICs. Therefore, it becomes increasingly difficult to fabricate a nanoscale IC with exact geometry. It results in considerable deviations of their performance. This deviation can cause logic failure that is caused by uncertainties in propagation delay from its mean value. Several sophisticated technology tools are required to observe the process induced parameter variations with shrinking device dimensions. Monte Carlo approach is implemented in order to study the impact of process variation on CNT based interconnects. This approach requires large numbers of simulation trials and is used to analyze the delay that is governed by the variability of process dependent parameters such as temperature, contact resistance, area and metallic ratio.

Depending on the geometry of SWCNT and MWCNT, this section presents the spatial and random arrangements of different CNT bundles. The bundle arrangements are used to model the interconnect parasitics of equivalent *RLC* circuit.

4.1 Process Induced Variation

In nanoscale regime, different process induced parameters such as bundle area, contact resistance, metallic ratio and temperature may have certain deviation in overall delay of interconnect. The variation in parameters primarily arises due to the difficulty in fabrication process and imperfect process control. Therefore, it is required to control the parameter that significantly affects the performance of an interconnect line. Process induced parameters are summarized in Table 4.1. Based on the variations, propagation delay deviation is analyzed for MCB, SWCNT bundle and MWCNT bundle having 3-, 5- and 10-shells, respectively.

Monte Carlo simulations are performed for 100 different samples with 30 distributed MTL network for SWCNT bundle, MWCNT bundle and MCB interconnects. It is intended to find the bundle that is more tolerant to the parasitic variation in terms of propagation delay and average deviation. It is observed that an MCB having randomly arranged CNTs provides improved performance as compared to the other CNT bundles. It is due to the presence of CNTs having different diameters that utilizes more bundle area.

Propagation delay obtained through simulations is verified against the analytical expression [20]. The analytical expression of 50% time delay, $\tau_{50\%}$ can be expressed as [20]

$$\tau_{50\%} = (1.48\zeta + e^{-2.9\zeta^{1.35}}) \sqrt{Ll(C'l + C_L)} \quad (38a)$$

where

$$\zeta = \frac{2(Rt + Rm)(C'l + C_L) + R'l(C'l + 2C_L)}{4\sqrt{Ll(C'l + C_L)}} \quad (38b)$$

R_t represents the input resistance of CMOS driver. Using the expression (20), it is observed that the analytical delay is in good agreement with the delay obtained through simulations as presented in Table 4.2.

However, the delay obtained through simulations exhibits an average error of 8.24% in comparison to the analytical delay.

Table 4.1 Parameter Variation/Range

Parameter	Nominal value	Variation/Range	Reference
Temperature	343.15	[293.4, 393.15]	[43]
Metallic ratio	1/3	30%	[43]
Contact resistance	5k Ω	50%	[43] [44]
Bundle area	2 μm^2 (sparsely packed) or 0.077 μm^2 (densely packed)	10% in width and 10% height	[43] [44]

Table 4.2 Propagation Delay for different CNT Bundles

Length (μm)	Propagation delay (ps)									
	Simulated					Analytical				
	SWCNT bundle	MWCNT bundle			MCB	SWCNT bundle	MWCNT bundle			MCB
	3 shell	5shell	10shell			3 shell	5 shell	10 shell		
100	66.00	39.18	30.749	20.93	7.38	66.79	39.058	29.24	19.576	5.225
500	380.60	197.04	139.46	85.016	9.951	405.65	208.96	146	87.22	8.3016
1000	960.22	457.02	310.88	179.05	13.22	1031.1	492.75	332.17	188.45	12.659

4.1.1 Temperature

Interconnects in VLSI circuits are prone to temperature variation due to on chip heat generation. It deviates the output voltage from its mean which causes an abnormal behaviour of logic circuits. Therefore, it is preferred to choose the interconnect bundle having minimum

average deviation. Fig. 4.1 presents the average deviation in delay for different CNT bundles at interconnect lengths ranging from 100 μm to 1000 μm .

It is observed that the average deviation in delay is significantly reduced for MCB as compared to the other CNT bundles. The mean free paths of CNTs are mainly affected by the temperature variation. The higher room temperature significantly reduces the mean free path that in turn increases the scattering resistance. Therefore, the delay deviation is mainly influenced by the variation of scattering resistance as presented in Table 4.3. Further observation reveals that using a densely packed MCB having CNTs with different diameters, one can obtain the minimum value of scattering resistance. Therefore, an MCB exhibits least deviation in delay as compared to other CNT bundles.

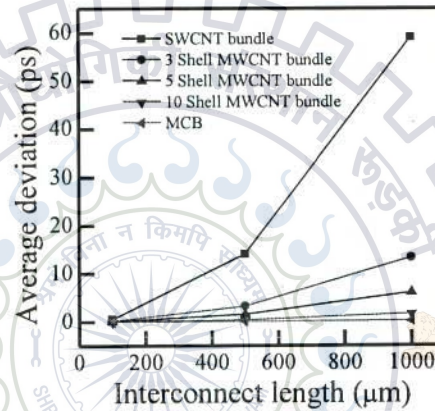


Figure 4.1 Average deviation in delay with different interconnect lengths for process induced temperature variation

Table 4.3 Interconnect parasitics for Process Induced Temperature variation

Parasitic	SWCNT Bundle	MWCNT bundle			MCB
		3 Shell	5 Shell	10 Shell	
$R_C(\Omega)$	[0.37, 0.33]	[0.41, 0.35]	[0.47, 0.39]	[0.57, 0.46]	[0.48, 0.40]
$R_{ST}(\Omega/\mu\text{m})$	[0.89, 1.7]	[0.56, 0.99]	[0.44, 0.75]	[0.29, 0.48]	[0.26, 0.44]
$L_{KT}(\text{pH}/\mu\text{m})$	[0.6, 0.53]	[0.66, 0.56]	[0.75, 0.63]	[1.02, 0.83]	[0.77, 0.64]
$L_{MT}(\text{pH}/\mu\text{m})$	[1.29, 1.29]	[1.11, 1.11]	[1.02, 1.02]	[0.9, 0.9]	[1.02, 1.02]
$C_{QT}(\text{pF}/\mu\text{m})$	[2.59, 2.9]	[2.34, 2.74]	[2.1, 2.5]	[1.7, 2.1]	[2.01, 2.42]
$C_E(\text{aF}/\mu\text{m})$	[1272, 1272]	[718.8, 71.88]	[521.4, 521.4]	[322.6, 322.6]	[10.9, 10.9]

4.1.2 Metallic ratio

In general, the metallic to semiconducting ratio for a CNT bundle is one-third. Depending on several fabrication limitations, it is quite difficult to achieve the exact ratio. Therefore, this research work takes into accounts the 30% deviation in the ratio as shown in Table 4.4. Using

different CNT bundles, the impact of metallic ratio on the average deviation in delay is shown in Fig. 4.2. It is observed that the impact of metallic ration on average deviation is almost 50% lesser in comparison to the process induced temperature variation. Variation in temperature has a major impact on mean free path and number of conducting channels while the metallic ration significantly affects the total number of conducting channels of a CNT bundle. The conducting channels considerably affects all the interconnect parasitics except magnetic inductance and electrostatic capacitance as seen in Table 4.4. Furthermore, it is observed that the variation in interconnect parasitics is minimum for MCB in comparison to the other CNT bundles. Therefore, an MCB exhibits lesser deviation in delay at different interconnect lengths.

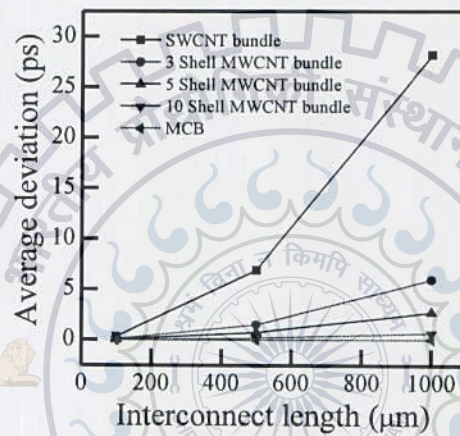


Figure 4.2 Average deviation in delay with different interconnect lengths for process induced metallic ration variation

Table 4.4 Interconnect Parasitics for Process Induced Metallic Ration variation

Parasitic	SWCNT bundle	MWCNT bundle			MCB
		3 Shell	5 Shell	10 Shell	
$R_C (\Omega)$	[0.53, 0.28]	[0.58, 0.31]	[0.66, 0.36]	[0.80, 0.43]	[0.68, 0.36]
$R_{ST} (\Omega/\mu\text{m})$	[1.36, 0.73]	[0.85, 0.46]	[0.66, 0.35]	[0.44, 0.24]	[0.39, 0.21]
$L_{KT} (\text{pH}/\mu\text{m})$	[0.85, 0.46]	[0.93, 0.50]	[1.06, 0.57]	[1.44, 0.77]	[1.1, 0.58]
$L_{MT} (\text{pH}/\mu\text{m})$	[1.29, 1.28]	[1.11, 1.11]	[1.02, 1.02]	[0.90, 0.90]	[1.02, 1.02]
$C_{QT} (\text{pF}/\mu\text{m})$	[1.83, 3.40]	[1.66, 0.31]	[1.46, 2.7]	[1.20, 2.23]	[1.43, 2.65]
$C_E (\text{fF}/\mu\text{m})$	[1.27, 1.27]	[0.72, 0.72]	[0.52, 0.52]	[0.32, 0.32]	[0.001, 0.001]

4.1.3 Contact resistance

Depending on the fabrication process, ambient temperature and technological parameters, contact resistance (R_C) of a CNT bundle varies in the range of 0 to 100k Ω . This research

work considers 50% variation in R_C as presented in Table 4.5. Using the process induced R_C variations, it is observed that the average deviation in delay is significantly reduced for MCB in comparison to the bundled SWCNT and bundled MWCNT as shown in Fig. 4.3. The densely packed arrangements of MCB are the primary reason behind this effect. The highly dense MCB consists of SWCNTs and MWCNTs of different diameters. The fabrication of R_C primarily controlled by the diameter of CNTs in a bundle. Therefore, different CNT diameters in MCB considerably reduces the delay performance at different interconnect lengths.

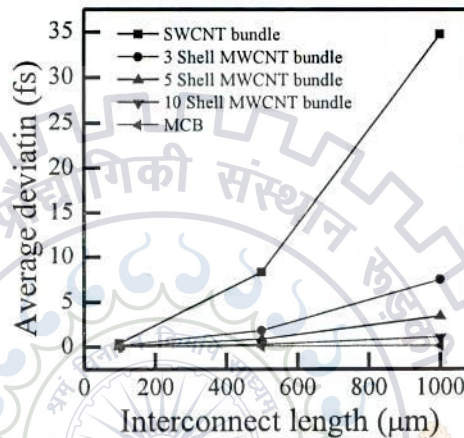


Figure 4.3 Average deviation in delay with different interconnect lengths for process induced contact resistance variation

Table 4.5 Interconnect parasitics for Process Induced contact resistance variation

Parasitics	SWCNT bundle	MWCNT bundle			MCB
		3 Shell	5 Shell	10 Shell	
$R_C(\Omega)$	[0.18,	[0.20, 0.61]	[0.23, 0.69]	[0.28, 0.84]	[0.24, 0.71]
$R_{ST}(\Omega/\mu\text{m})$	0.95	0.59	0.46	0.31	0.27
$L_{KT}(\text{pH}/\mu\text{m})$	0.59	0.65	0.74	1.00	0.75
$L_{MT}(\text{pH}/\mu\text{m})$	1.29	1.11	1.02	0.90	1.02
$C_{QT}(\text{pF}/\mu\text{m})$	0.26	2.4	2.1	1.72	2.0
$C_E(\text{fF}/\mu\text{m})$	1.27	0.72	0.52	0.32	1.09

4.1.4 Bundle Area

The area of a CNT bundle primarily depends on the bundle height and width. This research work considers a bundle area of $2\mu\text{m}^2$ (sparsely packed) and $0.077\mu\text{m}^2$ (densely packed) with 10% variation in bundle height and width (Table 4.1). Using the process induced bundle area

variations, the average deviation in delay with interconnect lengths is shown in Fig. 4.4. The higher bundle area significantly increases the number of CNTs that in turn reduces the interconnect parasitics. The variation of parasitics for different bundle area is presented in Table 4.6. It is observed that an MCB exhibits lesser variation in overall interconnect parasitics as compared to the other CNT bundles. Thus, MCB has lesser impact on the average deviation in delay in comparison to SWCNT and MWCNT bundles.

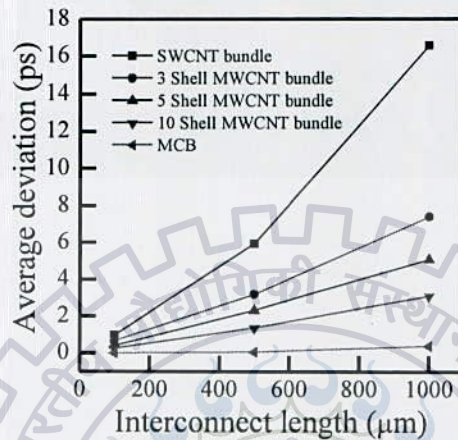


Figure 4.4 Average deviation in delay with different interconnect lengths for process induced bundle area variation

Table 4.6 Interconnect parasitics for Process Induced Bundle Area variation

Parasitics	SWCNT bundle	MWCNT bundle			MCB
		3 Shell	5 Shell	10 Shell	
$R_C(\Omega)$	[0.46, 0.31]	[0.50, 0.33]	[0.58, 0.38]	[0.70, 0.46]	[0.60, 0.39]
$R_{ST}(\Omega/\mu\text{m})$	[1.18, 0.79]	[0.73, 0.49]	[0.58, 0.38]	[0.40, 0.25]	[0.35, 0.23]
$L_{KT}(\text{pH}/\mu\text{m})$	[0.73, 0.49]	[0.81, 0.53]	[0.92, 0.61]	[1.26, 0.82]	[0.96, 0.63]
$L_{MT}(\text{pH}/\mu\text{m})$	[1.28, 1.29]	[1.11, 1.11]	[1.02, 1.02]	[0.90, 0.90]	[1.02, 1.02]
$C_{QT}(\text{pF}/\mu\text{m})$	[2.11, 3.14]	[1.92, 2.9]	[1.7, 2.55]	[1.37, 2.11]	[1.6, 2.5]
$C_E(\text{fF}/\mu\text{m})$	[1.143, 1.39]	[0.65, 0.8]	[0.47, 0.58]	[0.29, 0.36]	[1.09, 1.09]

5 Conclusion and Future work

5.1 Conclusion

In this dissertation report different aspect of interconnect parameters have been studied for different CNT bundles. Different modelling style has been proposed for MCB having different arrangements of CNTs so that performances parameters can be evaluated efficiently. These parameters involve delay, crosstalk and power dissipation that are compared for different CNT bundle to find the noble one. Model-I and Model-II is specifically designed to analyse the MCB with specific arranged CNTs whereas Model-III takes into account the MCB in which outer diameter of CNTs follows Gaussian distribution.

For specific arranged MCB, Model-I is implemented on bundled SWCNT, bundled MWCNT, MCB-I and MCB-II respectively. It is observed that MCB bundle are better as compared to others. MCB-II shows a significant improvement in crosstalk over bundled SWCNT, bundled MWCT and MCB-I with a maximum %age improvement of 89.36, 63.39 and 54.01 respectively whereas maximum improvement in power dissipation is recorded as 62.56, 59.88 and 57.10 respectively. On the other hand Model-II is implemented on MCB-III and MCB-IV. MCB-III is observed to be better than MCB-III with an average %age improvement in delay of 64.7%.

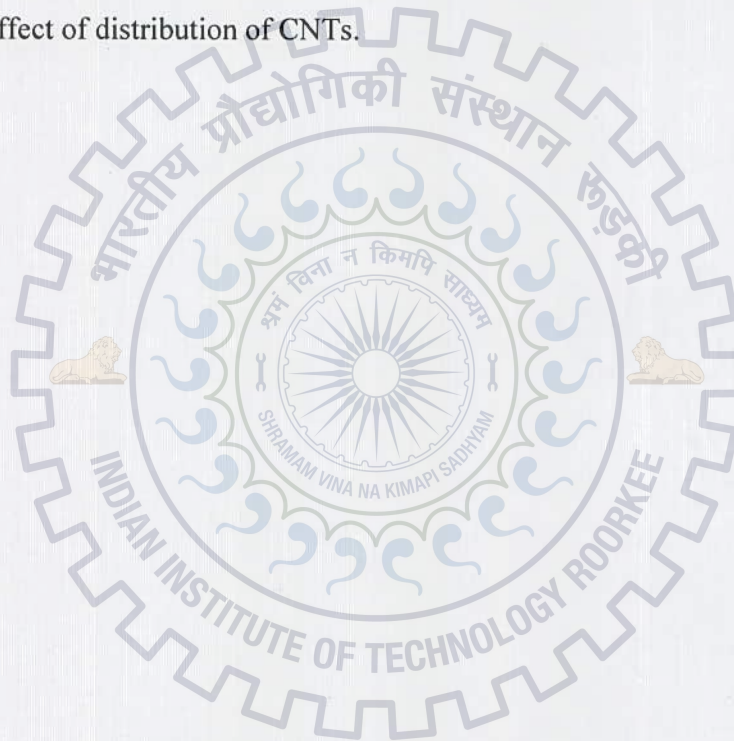
In order to analyse the performance of randomly arrangement of CNTs inside the bundle Model-III is used. It has been observed that MCB with higher tube density shows great improvement over the MCB with lower tube density in terms of delay and crosstalk. On the other hand due to increase in number of tubes for higher tube density power dissipation is increased but increment is not alarming.

Process induced variation such as temperature, bundle area, contact resistance and metallic ratio have been studied for MCB with randomly arranged bundle, MWCNT bundle with 5-, 10- and 15-shell and SWCNT respectively. Model-III is used for MCB and Model-II is used for other CNT bundles. It has been observed that MCB with random arrangement show a significant improvement in delay over other bundles. MCB is proved to be more tolerant to process induced variation as compared to others making MCB the best bundle to be used as VLSI interconnects.

5.2 Future work

The Model-I is designed to incorporate the bundle having specific arrangement of CNTs. This model is not general in the sense that it does not account for the different arrangement of CNTs within the bundle. So this model can be modified accordingly. On the other hand, Model-II is good enough to incorporate the CNTs arrangement inside the bundle but for this, arrangement of each CNT should be known beforehand which is a difficult task. This model has to be simplified as calculation in calculating equivalent capacitance is quite cumbersome.

Model-III as discussed efficiently models the randomly arranged MCB. This model does not account for the different distribution of CNTs within the bundle. This model can be modified to take the effect of distribution of CNTs.



References

- [1] S. Iijima, "Helical microtubules of graphite carbon," *Nature*, vol. 354, pp. 56-58, 1991.
- [2] Vladimir L. Kuznetsov, "Carbon 44," *ELSEVIER*, no. Boreskov Institute of Catalysis, Novosibirsk, Russia, 2006.
- [3] Peter J. F. Harris, *Carbon nanotubes and relayed structures: new materials for 21st century*. Cambridge, United Kingdom: Press syndicate of the university of cambridge, 1999.
- [4] Harold W. Kroto and David R.M. Walton. (2004) encyclopedia britannica: physical sciences, fullerene. [Online].
<http://www.britannica.com/EBchecked/topic/1566020/Physical-Sciences-Year-In-Review-2004>
- [5] Hong Li, Chuan Xu, Navin Srivastava, and Kaustav Banerjee, "Carbon Nanomaterials for Next-Generation Interconnects and Passives: Physics, Status, and Prospects," *IEEE TRANSACTIONS ON ELECTRON DEVICES*, vol. 56, no. 9, pp. 1799-1821, september 2009.
- [6] A. Nieuwoudt and Y. Massoud, "Assessing the Implications of Process Variations on Future Carbon Nanotube Bundle Interconnect Solutions," in *IEEE Computer Science*, 2007.
- [7] A. Jorio, G. Dresslehaus, and M. S. Dresselhaus, *Topics in applied physics*. Michigan, 2007.
- [8] J. Y. Hsieh, J. M. Lu, M. Y. Huang, and C. C. Hwang, "Softening phenomena of single-walled carbon nanotubes at higher temperature," *Banyan research express at NCKU*, vol. 1, no. 10, pp. 1-10, Oct 2007.
- [9] H. Li, W. Y. Yin, K. Banerjee, and J. F. Mao, "Circuit Modeling and Performance Analysis of Multi-Walled Carbon Nanotube Interconnects," *IEEE Trans. Electron Devices*, vol. 55, no. 6, pp. 1328-1337, Jun. 2008.
- [10] S. Subash, J. Kolar, and H. Masud, "A new spatially rearranged bundle of mixed carbon nanotubes as VLSI interconnect," *IEEE Trans. Nanotechnology*, vol. 12, no. 1, pp. 3-12, Jan. 2012.
- [11] Ji Yong Park, *Carbon Nanotube Electronics, Series on integrated circuits: Band Structure and Electron Transport Physics*. Korea: Springer science and business media, 2009.
- [12] B. Q. Wei, R. Vajtai, and P. M. Ajayan, "Reliability and current carrying capacity of carbon nanotubes," *Applied physics Letter*, vol. 79, no. 8, pp. 1172-1174, August 2001.
- [13] Hong Li, Chuan Xu, and Kaustav Banerjee, "Carbon Nanomaterials: The Ideal Interconnect technology for next generation ICs," *IEEE Design & Test of Computers*, vol. 27, no. 4, pp. 20-31, July 2010.
- [14] T. Ando, "The electronic properties of graphene and carbon nanotubes," *NPG Asian materials*, vol. 1, pp. 17-21, Oct. 2009.

- [15] (2008, november) cobweb. [Online]. <http://cobweb.ecn.purdue.edu/mdasilva/structure.html>
- [16] P. Avouris, M. Freitag, and V. Perbeinos, "Carbon nanotube photonics and optoelectronics," *Nature photonics*, vol. 2, pp. 341-350, 2008.
- [17] K. Donaldson et al., "Carbon Nanotubes: A Review of Their Properties in Relation to Pulmonary Toxicology and Workplace Safety," vol. 92, no. 1, pp. 5-22, Feb. 1996.
- [18] S. J. Tans, A. R. M. Verschueren, and C. Dekker, "Room-temperature transistor based on a single carbon nanotube," *Letters to nature*, vol. 393, no. 49, pp. 49-52, April 1998.
- [19] M. S. Dresselhaus, G. Dresselhaus, J. C. Charlier, and E. Hernandez, "Electronic, thermal and mechanical properties of carbon nanotubes," *Phil. Trans. R. Soc. Lond.*, vol. 362, pp. 2065-2098, August 2004.
- [20] T. R. Anthony et al., "Thermal conductivity of isotopically enriched ^{12}C diamond," *physics. rev.*, vol. 42, no. 2, pp. 1104-1111, 1989.
- [21] C. R. Hammond, *The Elements, in Handbook of Chemistry and Physics*, 81st ed.: CRC Press, June, 2006.
- [22] M. F. Yu, B. S. Files, S. Arepalli, and R. S. Ruoff, "Tensile Loading of Ropes of Single Wall Carbon Nanotubes and their Mechanical Properties," *in proc. Phys. Rev. Lett.*, vol. 84, no. 214, pp. 5552-5555, Jun. 2000.
- [23] D. A. Walters et al., "Elastic strain of freely suspended single-wall carbon nanotube ropes," *in proc. Appl. Phys. Lett.*, vol. 74, no. 25, Jun. 1999.
- [24] A. Jorio, G. Dresselhaus, and M. S. Dresselhaus, *Potential Applications of Carbon Nanotubes.*: Springer-Verlag Berlin Heidelberg, 2008.
- [25] (2005) International Technology Roadmap or Semiconductors. [Online]. <http://public.itrs.net>
- [26] M. P. A. Fisher and L. I. Glazman, "Transport in a one-dimensional Luttinger liquid," in *Mesoscopic Electron Transport*, dordrecht, The Netherlands: Kluwe, 1997.
- [27] N. Srivastava and K. Banerjee, "Interconnect challenges for nanoscale electronic circuits," *TMS J. Mater*, vol. 56, no. 10, pp. 30-31, 2004.
- [28] N. Srivastava and K. Banerjee, "A comparative scaling analysis of metallic and carbon nanotube interconnects for nanometer scale VLSI technologies," in *Int. VLSI Multilevel Interconnect Conf.*, 2004, pp. 393-398.
- [29] C. L. Cheung, A. Kurtz, H. Park, and C. M. Lieber, "Diameter-controlled synthesis of carbon nanotubes," *J. Phys. Chem.*, vol. 106, no. 10, pp. 2429-2433, Feb. 2002.
- [30] S. Harehanroengu and W. Wang., "Analyzing conductance of mixed carbon nanotube bundles for interconnect application," *IEEE Electron Device Lett.*, vol. 28, no. 8, pp. 756-759, Aug. 2007.
- [31] M. K. Majumder, N. D. Pandya, B. K. Kaushik, and S. K. Manhas, "Analysis of MWCNT and Bundled SWCNT Interconnects: Impact on Crosstalk and Area," *IEEE Electron Devices Letters*, vol. 33, no. 8, pp. 1180-1182, Aug. 2012.
- [32] S. N. Pu, W. Y. Yin, J. F. Mao, and Q. H. Liu, "Crosstalk Prediction of Single- and

- Double-Walled Carbon-Nanotube (SWCNT/ DWCNT) Bundle Interconnects," *IEEE Trans. Electron Devices*, vol. 56, no. 4, pp. 560-568, Apr. 2009.
- [33] P. J. Burke, "Luttinger Liquid Theory as a Model of the Gigahertz Electrical Properties of Carbon Nanotubes," *IEEE Trans. on Nanotech.*, vol. 1, no. 3, pp. 129-144, Sep. 2002.
- [34] "Modeling Crosstalk Effects in CNT Bus Architecture," *IEEE Trans. on Nanotechnol.*, vol. 6, no. 2, Mar. 2007.
- [35] A. Nieuwoudt and Y. Massoud, "Understanding impact of inductance in CNT bundles for VLSI interconnect using scalable modeling techniques," *IEEE Trans. Nanotech.*, vol. 5, no. 6, pp. 758-765, Nov. 2006.
- [36] H. J. Li., W. G. Lu, J. J. Li, X. D. Bai, and C. Z. Gu, "Multichannel ballistic transport in multiwall carbon nanotubes," *Phys. Rev. Lett.*, vol. 95, no. 8, pp. 086601-1-4, Aug. 2005.
- [37] W. Wang, S. Haruehanroengra, L. Shang, and M. Liu, "Inductance of mixed carbon nanotube bundles," *Micro and Nano Lett.*, vol. 2, no. 2, pp. 35-39, Jun. 2007.
- [38] B. S. Grewal, *Higher Engineering Mathematics*, 40th ed.: Khanna Publication, Jul. 2010.
- [39] M. D. Amore, M. S. Sarto, and A. Tamburrano, "Fast Transient Analysis of Next-Generation Interconnects Based on Carbon Nanotubes," *IEEE Trans. Electroman. Comput.*, vol. 52, no. 2, pp. 496-503, May 2010.
- [40] M. K. Majumder, N. D. Pandya, B. K. Kaushik, and S. K. Manhas, "Dynamic crosstalk effect in mixed CNT bundle interconnects," *IET Electronics Letters*, vol. 48, no. 7, pp. 384-385, Mar. 2012.
- [41] S. Sanvito, Y. K. Kwon, D. Tomanek, and C. J. Lambert, "Fractional Quantum Conductance in Carbon Nanotubes," *Phys. Rev. Lett.*, vol. 84, pp. 1974-1977, Feb. 2000.
- [42] P. Lamberti and V. Tucci, "Impact of the Variability of the Process Parameters on CNT-Based Nanointerconnects Performances: A Comparison Between SWCNTs Bundles and MWCNT," *IEEE Trans. Nanotechnol.*, vol. 11, no. 5, pp. 924-933, Sep. 2012.
- [43] A. Nieuwoudt and Y. Massoud, "On the Impact of Process Variations for Carbon Nanotube Bundles for VLSI Interconnect," *IEEE Trans. on electron devices*, vol. 54, no. 3, pp. 446-455, Mar. 2007.
- [44] Ali Keshavarzi and Arijit Raychowdhury, *Carbon nanotubes electronics, series on integrated circuit: Circuits, Applications and Outlook.*: Springer science and business media, 2009.
- [45] A. Naeemi and J. D. Meindl, "Compact physical models for multiwall carbon-nanotube interconnects," *IEEE Electorn Device Lett.*, vol. 27, no. 5, pp. 338-340, May 2006.
- [46] S. Datta, *Quantum Transport: From Atom to Transistor*. Cambridge, U.K.: Cambridge Press, 2005.

- [47] A. Nieuwoudt and Y. Massoud, "Evaluating the impact of resistance in carbon nanotube bundles for VLSI interconnect using diameter-dependent modeling techniques," *IEEE Trans. Electron Devices*, vol. 53, no. 10, pp. 2460-2466, Oct. 2006.
- [48] M. Nihei et al., "Novel approach to fabricate carbon nanotube via interconnects using size-controlled catalyst nanoparticles," in *Int. Interconnect Technol. Conf.*, Burlingame, Jun. 2006, pp. 230-232.



Publications

1. Jainender Kumar, Manoj Kumar Majumder, B.K. Kaushik and S. Dasgupta, "Analysis of Propagation Delay, Crosstalk and Power Dissipation in Randomly Arranged Mixed CNT Bundle Interconnects," *IEEE Trans. on computer aided desing of integrated circuit* (TCAD). (Communicated)
2. Jainender Kumar, Manoj Kumar Majumder, B.K. Kaushik and S. Dasgupta, "Process variation for different shell MWCNT bundle" in *Seventeenth International Symposium on VLSI Design and Test, 2013* (Accepted)
3. Jainender Kumar, Manoj Kumar Majumder, B.K. Kaushik, S. Dasgupta and S.K. Manhas, "Novel Modeling Approach to single and bundle MWCNT," in *Proc. IEEE International Conference on Communications, Devices and Intelligent Systems (CODIS)*, pp. 476-479, 2012.
4. Manoj Kumar Majumder, B. K. Kaushik, S. K. Manhas and Jainender Kumar, "Analysis of Crosstalk Delay and Power Dissipation in Mixed CNT Bundle Interconnects," in *Proc. IEEE International Conference on Communications, Devices and Intelligent Systems (CODIS)*, pp. 361-364, 2012.
5. Manoj Kumar Majumder, Jainender Kumar, B. K. Kaushik and S. K. Manhas, "Effect of intershell tunneling conductance in Multi-walled carbon nanotubes," in *Proc. National Conference on Research Trends in Communication Systems and devices*, RGGI Merrut Jul. 2012
6. Jainender Kumar, Manoj Kumar Majumder, B. K. Kaushik and S. Dasgupta, "Crosstalk analysis on Mixed CNT bundle," in *Proc. National Conference On Progress in Electronics & Allied Sciences, Gurukul Kangdi, Haridwar, Nov. 2012*

